Article

# IL-27 signalling promotes adipocyte thermogenesis and energy expenditure

https://doi.org/10.1038/s41586-021-04127-5

Received: 3 December 2018

Accepted: 13 October 2021

Published online: 24 November 2021

Check for updates

Qian Wang[1,2,17], Dehai Li[1,2,17], Guangchao Cao[1,2,17], Qiping Shi[3,17], Jing Zhu[1,2], Mingyue Zhang[1,2], Hao Cheng[4], Qiong Wen[1,2], Hao Xu[5], Leqing Zhu[2,6], Hua Zhang[1,2], Rachel J. Perry[7,8], Olga Spadaro[5,9], Yunfan Yang[9], Shengqi He[10], Yong Chen[10], Baocheng Wang[11], Guangqiang Li[2,6], Zonghua Liu[1,2], Caixian Yang[12], Xiaoli Wu[13], Libing Zhou[14], Qinghua Zhou[1,2], Zhenyu Ju[15], Hongyun Lu[1], Yongjie Xin[1], Xiaoyong Yang[8,9], Cunchuan Wang[16], Yong Liu[10], Gerald I. Shulman[7,8], Vishwa Deep Dixit[5,9], Ligong Lu[1,18] ✉, Hengwen Yang[1,2,18] ✉, Richard A. Flavell[5,18] ✉ & Zhinan Yin[1,2,18] ✉

Thermogenesis in brown and beige adipose tissue has important roles in maintaining body temperature and countering the development of metabolic disorders such as obesity and type 2 diabetes[1,2]. Although much is known about commitment and activation of brown and beige adipose tissue, its multiple and abundant immunological factors have not been well characterized[3–6]. Here we define a critical role of IL-27–IL-27Rα signalling in improving thermogenesis, protecting against diet-induced obesity and ameliorating insulin resistance. Mechanistic studies demonstrate that IL-27 directly targets adipocytes, activating p38 MAPK–PGC-1α signalling and stimulating the production of UCP1. Notably, therapeutic administration of IL-27 ameliorated metabolic morbidities in well-established mouse models of obesity. Consistently, individuals with obesity show significantly decreased levels of serum IL-27, which can be restored after bariatric surgery. Collectively, these findings show that IL-27 has an important role in orchestrating metabolic programs, and is a highly promising target for anti-obesity immunotherapy.

Chronic inflammation in times of nutritional excess has been proposed to be critical in regulating the development of obesity and metabolic syndrome[7,8]; however, the molecular factors that are involved have not been well defined. In an attempt to screen the inflammation-associated factors that are related to obesity, we determined the serum levels of different cytokines and found that the IL-12 family members (IL-27p28, IL-35 and IL-12p40) were significantly decreased in human participants with obesity (Extended Data Fig. 1a and Supplementary Table 1). Genome-wide association studies revealed that single-nucleotide polymorphisms in *IL27* (which encodes IL-27p28) are associated with body mass index (BMI)[9] and insulin resistance[10]. We therefore focused on the potential regulation of obesity by IL-27 signalling. IL-27 is a heterodimer composed of Epstein–Barr virus induced 3 (EBI-3) and p28, and regulates immune responses with pleiotropic effects[11]. We next examined the serum level of intact IL-27 using an enzyme-linked immunosorbent assay (ELISA) and found that it was indeed decreased in the group with obesity (Fig. 1a). Furthermore, the level of IL-27 further decreased as the degree of obesity increased (Extended Data Fig. 1b), and it was also inversely correlated with the fasting glucose levels of individuals with type 2 diabetes (Extended Data Fig. 1c and Supplementary Table 2). Interestingly, the IL-27 level of individuals with obesity was restored after bariatric surgery that reduced their body weight (Fig. 1b and Supplementary Table 3). These results strongly suggest that IL-27 signalling has a role in obesity and type 2 diabetes.

To investigate the role of IL-27 signalling in the development of obesity, we first fed IL-27Rα-deficient mice (*Il27ra*-knockout (KO) (also known as *Wsx1*-KO) mice) and C57BL/6J wild-type (WT) control mice with a high-fat diet (HFD). *Il27ra*-KO mice were highly susceptible to HFD-induced obesity (Fig. 1c, d and Extended Data Fig. 2a) and developed more severe glucose intolerance, insulin resistance (Fig. 1e–g) as well as steatohepatitis (Extended Data Fig. 2b, c). The serum levels of leptin and adiponectin in *Il27ra*-KO mice were increased (Extended Data Fig. 2d). Consistent with these metabolic phenotypes, HFD-fed *Il27ra*-KO mice also developed enhanced inflammatory responses in

[1]Guangdong Provincial Key Laboratory of Tumor Interventional Diagnosis and Treatment, Zhuhai Institute of Translational Medicine, Zhuhai People's Hospital Affiliated with Jinan University, Jinan University, Zhuhai, China. [2]The Biomedical Translational Research Institute, Faculty of Medical Science, Jinan University, Guangzhou, China. [3]Department of Endocrine, The First Affiliated Hospital, Jinan University, Guangzhou, China. [4]Key Laboratory for the Genetics of Developmental & Neuropsychiatric Disorders (Ministry of Education), Bio-X Institutes, Shanghai Jiao Tong University, Shanghai, China. [5]Department of Immunobiology, School of Medicine, Yale University, New Haven, CT, USA. [6]The First Affiliated Hospital, Faculty of Medical Science, Jinan University, Guangzhou, China. [7]Department of Medicine, School of Medicine, Yale University, New Haven, CT, USA. [8]Department of Cellular & Molecular Physiology, School of Medicine, Yale University, New Haven, CT, USA. [9]Department of Comparative Medicine, School of Medicine, Yale University, New Haven, CT, USA. [10]Hubei Key Laboratory of Cell Homeostasis, College of Life Sciences, Institute for Advanced Studies, Wuhan University, Wuhan, China. [11]Tsinghua Berkeley Shenzhen Institute (TBSI), Tsinghua University, Shenzhen, China. [12]Department of Endocrine, The Sixth Affiliated Hospital of Guangzhou Medical University, Qingyuan People's Hospital, Qingyuan, China. [13]School of Life Sciences, Tianjin University, Tianjin, China. [14]Guangdong-Hong Kong-Macau Institute of CNS Regeneration, Ministry of Education CNS Regeneration Collaborative Joint Laboratory, Jinan University, Guangzhou, China. [15]Key Laboratory of Regenerative Medicine of Ministry of Education, Institute of Aging and Regenerative Medicine, Jinan University, Guangzhou, China. [16]Department of Surgery, The First Affiliated Hospital of Jinan University, Guangzhou, China. [17]These authors contributed equally: Qian Wang, Dehai Li, Guangchao Cao, Qiping Shi. [18]These authors jointly supervised this work: Ligong Lu, Hengwen Yang, Richard A. Flavell, Zhinan Yin. ✉e-mail: lu_ligong@163.com; hengwenyang@jnu.edu.cn; richard.flavell@yale.edu; tzhinan@jnu.edu.cn

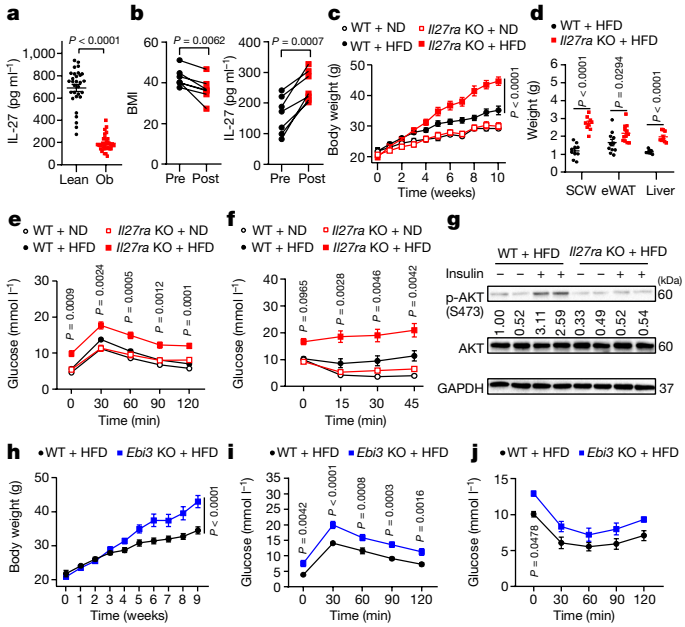

**Fig. 1 | IL-27 restrains the development of obesity and insulin resistance.** **a**, The serum levels of IL-27 in individuals with obesity (Ob) ($n = 32$) and control individuals with a healthy BMI (lean) ($n = 30$). **b**, The BMI and serum IL-27 level of patients with obesity before (pre) and one month after (post) gastric bypass surgery. $n = 7$. **c**–**g**, *Il27ra*-KO mice and WT controls (aged 8 weeks) were treated with an HFD or ND for 10 weeks. **c**, Body weight was recorded each week. $n = 5$ (WT, ND), $n = 6$ (WT, HFD; and KO, ND) and $n = 7$ (KO, HFD). **d**, Tissues were collected and weighed. $n = 10$ (WT, SCW and liver), $n = 9$ (KO, SCW and liver) $n = 11$ (WT, epididymal white adipose tissue (eWAT)) and $n = 12$ (KO, eWAT). **e**, **f**, Intraperitoneal glucose tolerance test (GTT) (**e**; $n = 6$ (ND), $n = 5$ (KO, HFD) and $n = 4$ (WT, HFD)) and insulin tolerance test (ITT) (**f**; $n = 5$ (WT, ND), $n = 6$ (WT, HFD; and KO, ND) and $n = 7$ (KO, HFD). **g**, HFD-fed WT and *Il27ra*-KO mice (10 weeks) were tested for insulin sensitivity through immunoblot analysis of phosphorylated AKT (p-AKT S473) in epididymal fat. **h**–**j**, *Ebi3*-KO mice and WT controls (aged 8 weeks) were treated with an HFD for 9 weeks. **h**, Body weights were recorded each week. $n = 6$ (WT) and $n = 5$ (KO). **i**, **j**, GTT (**i**) and ITT (**j**) analyses were performed. $n = 8$ (WT) and $n = 4$ (KO). Data are mean ± s.e.m. of biologically independent samples. Statistical analysis was performed using two-tailed unpaired Student's *t*-tests (**a** and **d**), two-tailed paired Student's *t*-tests (**b**), two-way analysis of variance (ANOVA) (**c** and **h**) and two-way ANOVA with Sidak's multiple-comparisons test (**e**–**f** and **i**–**j**).

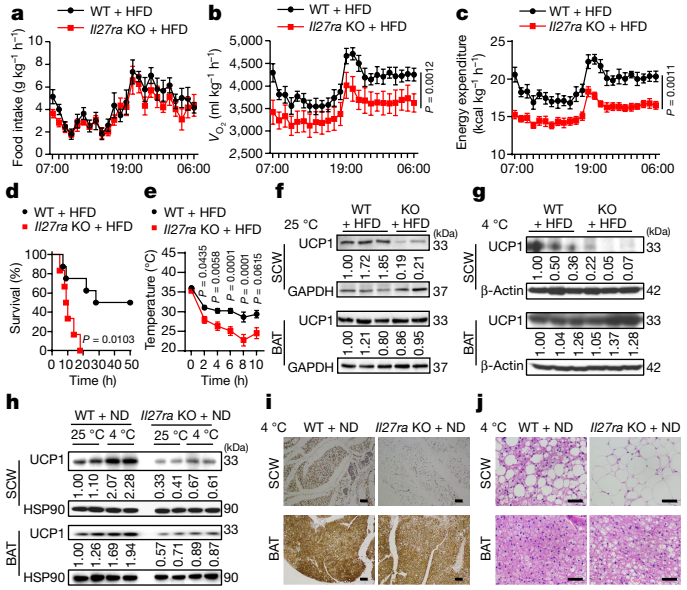

**Fig. 2 | IL-27 signalling promotes thermogenesis and energy expenditure.** **a**–**c**, *Il27ra*-KO and WT mice were fed an HFD for 4 weeks and then placed into metabolic cages. Food intake (**a**; $n = 7$), oxygen consumption ($V_{O_2}$; **b**; $n = 7$ (WT) and $n = 8$ (KO)) and energy expenditure (**c**; $n = 7$ (WT) and $n = 8$ (KO)) were monitored over a 24 h period. **d**, **e**, *Il27ra*-KO and WT mice were fed an HFD for 6 weeks and then cold challenged at 4 °C. The survival curve (**d**; $n = 8$ (WT) and $n = 6$ (KO)) and rectal temperature (**e**; $n = 15$ (WT) and $n = 11$ (KO)) are shown. **f**, **g**, *Il27ra*-KO and WT mice were fed an HFD for 6 weeks and then housed at 25 °C (**f**) or challenged at 4 °C for 2 h (**g**). SCW and BAT samples were collected for immunoblot analysis of UCP1. **h**–**j**, *Il27ra*-KO and WT mice fed a ND were housed at 25 °C or cold challenged at 4 °C for 48 h. **h**, SCW and BAT samples were collected for immunoblot analysis of UCP1. **i**, Immunohistochemical staining of UCP1. Scale bars, 100 μm. **j**, Haematoxylin and eosin (H&E) staining of BAT and SCW tissues. Scale bars, 50 μm. Data are mean ± s.e.m. of biologically independent samples. Statistical analysis was performed using two-way ANOVA (**a**–**c**), two-way ANOVA with Sidak's multiple-comparisons test (**e**) and log-rank tests (**d**).

adipose tissue, as indicated by increased macrophage infiltration and higher inflammatory cytokine production (Extended Data Fig. 2e, f). As *Il27ra*-KO mice have an approximately C57BL6/NJ genotype, we also used C57BL/6N WT mice as the control group and observed similar phenotypes (Extended Data Fig. 2g–j). Even *Il27ra*$^{+/-}$ heterozygote mice showed considerably increased body weight and impaired insulin sensitivity after feeding on an HFD, suggesting a dose-dependent effect of IL-27 signalling (Extended Data Fig. 2k–n). Interestingly, glucose metabolism was already impaired in *Il27ra*-KO mice after 4 weeks of HFD feeding (Extended Data Fig. 2o), despite the fact that no significant difference in body weight was observed compared with the WT controls at this time (Fig. 1c). This suggests that there was a precommitted metabolic alteration after IL-27 signalling deficiency. Moreover, we also found that mice that were deficient in EBI-3 were more susceptible to HFD-induced obesity and glucose intolerance (Fig. 1h–j). Collectively, these results strongly demonstrate a protective role of IL-27 signalling in restraining obesity and related metabolic morbidities.

We next examined whether IL-27 signalling deficiency affects energy balance. *Il27ra*-KO mice that were maintained on a normal diet (ND) showed significantly reduced energy expenditure without altered food intake (Extended Data Fig. 3a–c). The phenotype was even more striking when they were fed an HFD (Fig. 2a–c). An analysis of adipose tissues revealed reduced oxygen consumption (Extended Data Fig. 3d), indicating a promoting action of IL-27 signalling in maintaining energy homeostasis. To determine the molecular mechanisms that underlie the impairment of energy expenditure after IL-27Rα deficiency, we performed a transcriptomic analysis of subcutaneous white adipose tissue (SCW) from HFD-fed *Il27ra*-KO or WT mice. Gene set enrichment analysis revealed that IL-27Rα deficiency resulted in alterations in multiple cellular functions and signalling pathways (Supplementary Table 4), including significant impairment of the brown/beige adipocyte thermogenesis program and PPAR signalling pathway (Extended Data Fig. 3e, f). A reduced expression of several thermogenic genes in *Il27ra*-KO mice was detected even in mice that were fed a ND (Extended Data Fig. 3g).

Brown/beige adipocyte thermogenesis has a key role in driving energy expenditure that has increasingly been considered to be a target for combating the development of obesity and metabolic syndrome[1,2]. To determine whether the effect of IL-27Rα deficiency on energy expenditure is attributable to decreased heat production, we next analysed adaptive thermogenesis. Consistent with their increased susceptibility to diet-induced obesity, *Il27ra*-KO mice were hypersensitive to cold-induced hypothermia when fed the ND (Extended Data Fig. 3h, i), and this cold intolerance was even more severe after HFD feeding (Fig. 2d, e). Consistently, expression of uncoupling protein 1 (UCP1), the key mitochondrial protein in thermogenesis, was also markedly reduced in the SCW of *Il27ra*-KO mice that were fed the HFD

or ND, either after being maintained at 25 °C or after cold exposure at 4 °C (Fig. 2f–i). Histological analyses also showed less cells with multilocular lipid droplets (Fig. 2j) in the SCW of *Il27ra*-KO mice. The reduction of UCP1 in the brown adipose tissues (BAT) was either less substantial (Fig. 2h) or largely unchanged (Fig. 2f, g), suggesting that the effect of IL-27 signalling on the thermogenesis program occurred mainly through actions in the SCW, and presumably IL-27 regulates beige adipocytes more robustly than brown adipocytes. Note that UCP1 was already decreased in *Il27ra*-KO mice without cold stimulation (Fig. 2f, h), which was in accordance with the decreased systemic energy expenditure (Fig. 2b, c and Extended Data Fig. 3b, c). Moreover, a cold challenge test in *Ebi3*-KO mice recapitulated the findings in *Il27ra*-KO mice (Extended Data Fig. 3j–l), and supplementing IL-27 in *Ebi3*-KO mice upregulated UCP1 and ameliorated the cold-induced hypothermia (Extended Data Fig. 3m–p), further verifying the thermogenic effects of IL-27 signalling.

Previous studies showed that immune cells, especially lymphoid lineage cells, express high levels of IL-27R[11] and the immune system was known to be involved in the development of obesity[7]. We therefore next investigated whether IL-27 regulates the development of obesity through actions on these immune cells. We generated *Il27ra*$^{flox/flox}$ mice (Extended Data Fig. 4a–c) and crossed them with *Cd2-cre* or *Lyz2-cre* mice to specifically delete *Il27ra* in lymphoid cells (T cells and B cells) or myeloid cells (monocytes, mature macrophages and granulocytes), respectively (Extended Data Fig. 4d). Surprisingly, deficiency of IL-27Rα in these cells did not alter their susceptibility to HFD-induced obesity or the related metabolic syndrome (Extended Data Fig. 4e–h). To determine which cell types were responsible for IL-27-mediated signalling in obesity, we generated four groups of chimera mice (bone marrow from WT mice in WT mice (WT > WT), WT > KO, KO > WT and KO > KO) using bone marrow from *Il27ra*-KO or WT mice and fed these mice an HFD. Interestingly, only those chimeras that were prepared using *Il27ra*-KO recipient mice regardless of the donor cells were highly susceptible to HFD-induced obesity and metabolic syndrome (Fig. 3a and Extended Data Fig. 5a–d). Consistently, the thermogenesis of WT > KO chimeras was dampened compared with WT > WT chimeras as indicated by lower hypothermia, less multilocular lipid droplets and reduced expression of UCP1 in the SCW (Fig. 3b, c and Extended Data Fig. 5e–g). These results strongly suggest that the dominant targets of IL-27 signalling in mediating metabolic homeostasis were not radiation-sensitive immune cells. Direct actions of IL-27 on non-immune cells were reported recently[12] and *Il27ra* transcripts were also detected in adipocytes[13]. Indeed, IL-27Rα protein was detectable in the adipocyte fraction of adipose tissues as well as in in vitro-differentiated primary beige adipocytes (Extended Data Fig. 6a, b). The expression of IL-27Rα in the SCW was much higher than that in the BAT, which coincided with more striking phenotypes in the SCW. To test whether IL-27 could directly target adipocytes to regulate thermogenesis and obesity, we crossed *Il27ra*$^{flox/flox}$ mice with *Adipoq-cre* mice to specifically delete *Il27ra* in adipocytes (Extended Data Fig. 6c, d). Abolishing IL-27Rα signalling in adipocytes predisposed the mice to hypersensitivity to HFD-induced obesity and the related metabolic syndrome (Fig. 3d and Extended Data Fig. 6e–k), which recapitulated our findings in mice with a global KO of *Il27ra*. Furthermore, the thermogenesis of *Adipoq-cre*;*Il27ra*$^{flox/flox}$ mice was also dampened as indicated by intolerance to cold challenge, decreased UCP1 expression and less multilocular lipid droplets in the SCW (Fig. 3e, f and Extended Data Fig. 6l, m). As *Adipoq-cre*;*Il27ra*$^{flox/flox}$ deletes *Il27ra* in all fat cells, we also examined whether IL-27Rα signalling in beige/brown adipocytes could regulate thermogenesis by crossing *Il27ra*$^{flox/flox}$ with *Ucp1-creERT2* mice to specifically delete *Il27ra* in beige/brown adipocytes after tamoxifen induction. Given that UCP1 is expressed in most adipocytes in early adipose tissue development[14], we used this inducible conditional KO strain rather than *Ucp1-cre* to avoid possible developmental effects. *Ucp1-creERT2*;*Il27ra*$^{flox/flox}$ mice were also more sensitive to HFD-induced obesity (Fig. 3g and Extended Data Fig. 7a–c) and cold-induced hypothermia (Fig. 3h, i and Extended Data Fig. 7d) compared with tamoxifen-treated *Il27ra*$^{flox/flox}$ control mice, although the differences were less substantial compared with in *Adipoq-cre*;*Il27ra*$^{flox/flox}$ mice (Fig. 3d and Extended Data Fig. 6f, g) or mice with a global KO of *Il27ra* (Fig. 1c–f). The diminished phenotypes in *Ucp1-creERT2*;*Il27ra*$^{flox/flox}$ mice might be due to the reduced but not complete loss of IL-27Rα in the SCW adipocyte fraction (as not all adipocytes express UCP1; Extended Data Fig. 7a), which suggests that expression of IL-27Rα in UCP1$^{low}$ or UCP1$^{-}$ adipocytes also has an important role in these processes. Collectively, these data clearly demonstrate that IL-27 directly targets adipocytes to promote thermogenesis and protect against obesity, with beige/brown adipocytes serving as important responders.

To dissect the molecular mechanism by which IL-27 regulates thermogenic adipocytes, we directly treated primary beige adipocytes with IL-27 in vitro. The expression of UCP1 was substantially increased after IL-27 treatment, together with upregulated peroxisome proliferator-activated receptor alpha (PPARα) and peroxisome proliferator-activated receptor gamma co-activator 1alpha (PGC-1α), the two key transcriptional activators that govern the energy metabolism[15,16] (Fig. 4a and Extended Data Fig. 7e). The canonical downstream signalling pathways of IL-27Rα are mediated by STAT1, STAT3 and p38

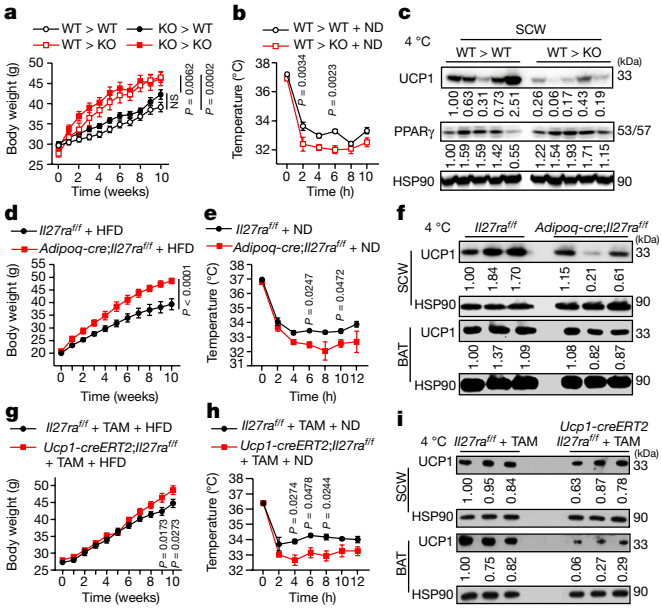


**Fig. 3 | IL-27 directly targets adipocytes to promote thermogenesis and combat obesity. a**, Four groups of bone marrow chimeras were generated using *Il27ra*-KO or WT mice and fed an HFD for 10 weeks. The body weights were recorded weekly. $n = 14$ (WT > WT), $n = 11$ (WT > KO), $n = 12$ (KO > WT), $n = 10$ (KO > KO). NS, not significant. **b**, The rectal temperature of chimeric mice fed normal chow in response to a cold challenge at 4 °C. $n = 7$ (WT > WT) and $n = 6$ (WT > KO). **c**, After the cold challenge for 12 h, SCW samples were collected for immunoblot analysis. **d**, *Adipoq-cre*;*Il27ra*$^{flox/flox}$ ($n = 7$) and *Il27ra*$^{flox/flox}$ ($n = 9$) mice (aged 8 weeks) were fed an HFD for 10 weeks. Body weight was recorded weekly. **e**, The rectal temperature of mice fed an ND in response to cold challenge at 4 °C. $n = 16$ (*Il27ra*$^{flox/flox}$) and $n = 17$ (*Adipoq-cre*;*Il27ra*$^{flox/flox}$). **f**, After the cold challenge for 12 h, SCW and BAT samples were collected for immunoblot analysis. **g**, *Ucp1-creERT2*;*Il27ra*$^{flox/flox}$ ($n = 12$) and *Il27ra*$^{flox/flox}$ ($n = 11$) mice (aged 8 weeks) were pretreated with tamoxifen and then fed an HFD for 10 weeks. Body weight was recorded weekly. **h**, The rectal temperature of mice fed an ND in response to cold challenge at 4 °C. $n = 4$ (*Il27ra*$^{flox/flox}$) and $n = 6$ (*Ucp1-creERT2*;*Il27ra*$^{flox/flox}$). **i**, After the cold challenge for 12 h, SCW and BAT samples were collected for immunoblot analysis. Data are mean ± s.e.m. of biologically independent samples. Statistical analysis was performed using two-way ANOVA (**a** and **d**) and two-way ANOVA with Sidak's multiple-comparisons test (**b**, **e**, **g** and **h**).

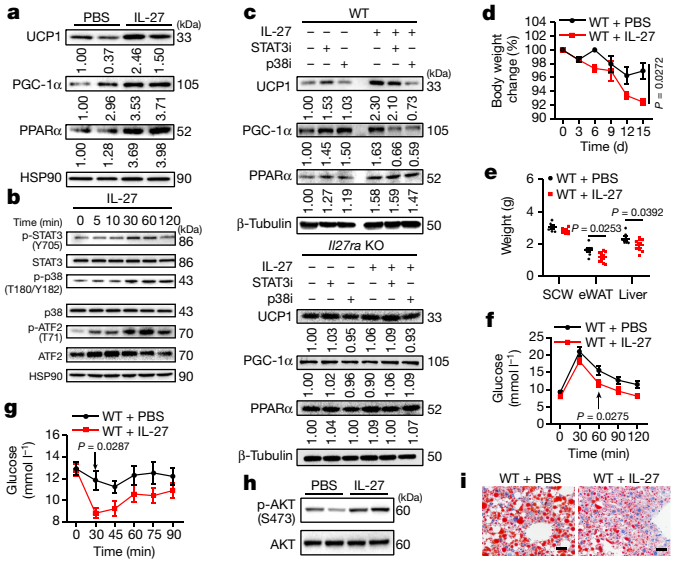


**Fig. 4 | IL-27 promotes the activation of thermogenesis with promising therapeutic potential. a**, Primary beige adipocytes were generated in vitro from the stromal vascular fraction of WT SCW, treated with rmIL-27 (100 ng ml$^{-1}$) or PBS for 24 h and used for immunoblotting analysis. **b**, Immunoblotting analysis of protein phosphorylation of WT primary beige adipocytes in response to treatment with rmIL-27 (100 ng ml$^{-1}$). **c**, Primary beige adipocytes from WT and *Il27ra*-KO SCW samples were generated in vitro. Cells were treated with STAT3 inhibitor (STAT3i; C188-9, 10 μM) or p38 MAPK inhibitor (p38i; SB203580, 10 μM) and used for immunoblotting analysis of the interested proteins. **d**–**i**, WT mice were fed an HFD for 32 weeks and then intraperitoneally injected with rmIL-27 (100 μg kg$^{-1}$) or PBS every other day for 15 d. **d**, Body weight was recorded at indicated time points. $n = 8$. **e**–**g**, Tissues were weighed (**e**; $n = 6$ (SCW), $n = 8$ (eWAT), $n = 7$ (liver, PBS) and $n = 8$ (liver, IL-27)), and GTT (**f**; $n = 12$ (PBS) and $n = 11$ (IL-27)) and ITT (**g**; $n = 9$ (PBS) and $n = 8$ (IL-27)) measurements were performed, after 15 d treatment. **h**, Immunoblotting analysis of phosphorylated AKT (p-AKT S473) in eWAT was performed for insulin sensitivity analysis and shown. **i**, Oil red O staining of liver tissues after rmIL-27 therapy for 15 d. Scale bars, 50 μm. Data are mean ± s.e.m. of biologically independent samples. Statistical analysis was performed using two-tailed unpaired student's *t*-tests (**e**), two-way-ANOVA (**d**) and two-way ANOVA with Sidak's multiple-comparisons test (**f** and **g**).

MAPK in immune cells[11,17]. We next determined whether IL-27 promotes the activation of thermogenesis in adipocytes through these pathways. The phosphorylation of p38 MAPK was significantly increased after IL-27 stimulation, and the phosphorylation activation of STAT3 was only transiently induced and rapidly faded, while the phosphorylation of STAT1 was barely detectable (Fig. 4b and Extended Data Fig. 7f). It is well established that p38 MAPK instigates ATF2-mediated upregulation of PGC-1α—the master regulator of UCP1 and thermogenesis[15,16,18,19]. Indeed, IL-27 treatment augmented ATF2 activation in primary beige adipocytes with ensuing upregulation of PGC-1α, which could be abrogated by pharmacological inhibition of the activity of p38 MAPK (Fig. 4a–c). Moreover, cells with p38 MAPK inhibition were refractory to IL-27 induced promotion of UCP1 expression (Fig. 4c and Extended Data Fig. 7g, h). However, IL-27 upregulation of UCP1 was largely unaffected in response to STAT3 inhibition, even though it also decreased PGC-1α expression (Fig. 4c and Extended Data Fig. 7g, h). These phenomena disappeared when the IL-27 treatment was performed in *Il27ra*-KO mouse primary beige cells (Fig. 4c). These results indicate that IL-27 could promote the activation of thermogenesis mainly through the p38 MAPK–PGC-1α signalling pathway. Interestingly, neither p38 MAPK nor STAT3 inhibition abrogated the upregulation of PPARα by IL-27 (Fig. 4c (top)), suggesting additional pathways might be involved in mediating IL-27 actions. An unexpected upregulation of PGC-1α was detected after treatment with the STAT3 inhibitor or p38 inhibitor alone in the absence of IL-27 stimulation, and STAT3 inhibitor alone appeared to slightly increase UCP1 expression (Fig. 4c and Extended Data Fig. 7h), suggesting that STAT3 and p38 MAPK might have complicated actions in thermogenesis under unstimulated conditions.

As IL-27 signalling promotes thermogenesis and restrains obesity, and individuals with obesity showed significantly decreased serum IL-27 levels (Fig. 1a), we next sought to test whether IL-27 has therapeutic potential. We treated obese WT mice with IL-27 and observed significantly reduced body weight and adipose deposition (Fig. 4d, e). More importantly, IL-27 administration also substantially ameliorated insulin resistance and hepatic steatosis (Fig. 4f–i). These findings revealed a strong therapeutic potential of triggering the IL-27 signalling pathway for the treatment of obesity and insulin resistance. We also applied IL-27 therapy to obese *Il27ra*$^{flox/flox}$, *Adipoq-cre*;*Il27ra*$^{flox/flox}$, *Ucp1-creERT2*;*Il27ra*$^{flox/flox}$ and *Ucp1*-KO mice. IL-27 injection did not cause systemic inflammation or tissue damage (Extended Data Fig. 8a–c). Consistent with the findings in WT mice, IL-27 administration also significantly reduced the body weight and improved glucose metabolism in *Il27ra*$^{flox/flox}$ control mice (Extended Data Fig. 8d–f). By contrast, the protective effects of IL-27 therapy vanished in *Adipoq-cre*;*Il27ra*$^{flox/flox}$ and *Ucp1*-KO mice, and diminished in *Ucp1-creERT2*;*Il27ra*$^{flox/flox}$ mice (Extended Data Fig. 8g–p). These data indicate that the beneficial effects of IL-27 treatment depend on its actions on adipocytes, with beige/brown adipocytes as the key responders. The protective effects of IL-27 therapy in *Ucp1-creERT2*;*Il27ra*$^{flox/flox}$ mice were not completely abolished as in *Adipoq-cre*;*Il27ra*$^{flox/flox}$ mice (Extended Data Fig. 8g–l), suggesting again that IL-27Rα signalling in additional types of adipocytes might also have an important role in these processes. The loss of the therapeutic effects of IL-27 in obese *Ucp1*-KO mice (Extended Data Fig. 8m–p) suggested that UCP1 is required for the metabolic improvement by IL-27.

Myeloid cells such as macrophages and dendritic cells are important IL-27 producers[11], and the expression of IL-27 in adipocytes was also reported previously[13]. We next investigated whether the IL-27 was produced from these cells to restrain obesity. We crossed *Il27p28*$^{flox/flox}$ mice with *Lyz2-cre*, *Itgax-cre* or *Adipoq-cre* mice to specifically eliminate the production of IL-27 from monocytes, mature macrophages and granulocytes; dendritic cells and M1 macrophages; or adipocytes, respectively, and challenged these mice with an HFD. Unexpectedly, none of these mice recapitulated the findings in IL-27Rα-deficient or *Ebi3*-KO mice (Extended Data Fig. 9a–i). We next sought to test whether the source of IL-27 in the adipose tissue might be CX3CR1$^{+}$ cells, which contain sympathetic-neuron-associated macrophages that regulate thermogenesis and accumulate in obesity[20]. *Cx3cr1-cre*;*Il27p28*$^{flox/flox}$ mice showed a tendency to gain more weight after feeding with an HFD (Extended Data Fig. 9j). More importantly, these mice displayed worse glucose intolerance and insulin resistance after 10 weeks of HFD feeding (Extended Data Fig. 9k, l), indicating that CX3CR1$^{+}$ cells may represent an important source of IL-27 in combating obesity. As the CX3CR1$^{+}$ cohorts are very complicated[21], the precise cell types of these CX3CR1$^{+}$ cells remain to be delineated. Besides, the increase of body weight after IL-27p28 deletion in CX3CR1$^{+}$ cells was much less substantial than that in IL-27Rα- or EBI-3-deficient mice (Extended Data Fig. 9j), suggesting that there might be other sources of IL-27 that also contribute to obesity regulation. Inflammatory cytokines such as IFNs and TLR ligands such as LPS are known to stimulate the production of IL-27 (ref. [11]), but whether these signals are involved in affecting the production of IL-27 or IL-27-producing cells during obesity-related metabolic inflammation needs further investigation.

In summary, our studies have uncovered that IL-27 signalling is required for intact adaptive thermogenesis and systemic metabolic homeostasis. IL-27 directly targets adipocytes to elicit the activation of p38 MAPK, thereby driving the activation of ATF2 and the ensuing expression of PGC-1α and UCP1. Importantly, administration of IL-27

ameliorates obesity and insulin resistance in mice, and reduced serum IL-27 is correlated with the development of obesity in humans. Taken together, these findings provide new insights into IL-27 biology, expand our understanding of thermogenic control, and reveal IL-27 as a biologic agent with promising potential for anti-obesity immunotherapy.

## Online content

Any methods, additional references, Nature Research reporting summaries, source data, extended data, supplementary information, acknowledgements, peer review information; details of author contributions and competing interests; and statements of data and code availability are available at https://doi.org/10.1038/s41586-021-04127-5.


1. Betz, M. J. & Enerback, S. Human brown adipose tissue: what we have learned so far. *Diabetes* **64**, 2352–2360 (2015).
2. Bartelt, A. & Heeren, J. Adipose tissue browning and metabolic health. *Nat. Rev. Endocrinol.* **10**, 24–36 (2014).
3. Wang, W. & Seale, P. Control of brown and beige fat development. *Nat. Rev. Mol. Cell Biol.* **17**, 691–702 (2016).
4. Odegaard, J. I. et al. Perinatal licensing of thermogenesis by IL-33 and ST2. *Cell* **166**, 841–854 (2016).
5. Qiu, Y. et al. Eosinophils and type 2 cytokine signaling in macrophages orchestrate development of functional beige fat. *Cell* **157**, 1292–1308 (2014).
6. Camell, C. D. et al. Inflammasome-driven catecholamine catabolism in macrophages blunts lipolysis during ageing. *Nature* **550**, 119–123 (2017).
7. Reilly, S. M. & Saltiel, A. R. Adapting to obesity with adipose tissue inflammation. *Nat. Rev. Endocrinol.* **13**, 633–643 (2017).
8. Lackey, D. E. & Olefsky, J. M. Regulation of metabolism by the innate immune system. *Nat. Rev. Endocrinol.* **12**, 15–28 (2016).
9. Hoffmann, T. J. et al. A large multiethnic genome-wide association study of adult body mass index identifies novel loci. *Genetics* **210**, 499–515 (2018).
10. Vargas-Alarcon, G. et al. Interleukin 27 polymorphisms, their association with insulin resistance and their contribution to subclinical atherosclerosis. The GEA Mexican study. *Cytokine* **114**, 32–37 (2019).
11. Yoshida, H. & Hunter, C. A. The immunobiology of interleukin-27. *Ann. Rev. Immunol.* **33**, 417–443 (2015).
12. Yang, B. et al. IL-27 facilitates skin wound healing through induction of epidermal proliferation and host defense. *J. Invest. Dermatol.* **137**, 1166–1175 (2017).
13. Nam, H., Ferguson, B. S., Stephens, J. M. & Morrison, R. F. Modulation of IL-27 in adipocytes during inflammatory stress. *Obesity* **24**, 157–166 (2016).
14. Wolfrum, C. & Straub, L. G. Lessons from Cre-mice and indicator mice. *Handb. Exp. Pharmacol.* **251**, 37–54 (2019).
15. Kissig, M., Shapira, S. N. & Seale, P. SnapShot: brown and beige adipose thermogenesis. *Cell* **166**, 258–258 (2016).
16. Kajimura, S. & Saito, M. A new era in brown adipose tissue biology: molecular control of brown fat development and energy homeostasis. *Ann. Rev. Physiol.* **76**, 225–249 (2014).
17. Owaki, T., Asakawa, M., Fukai, F., Mizuguchi, J. & Yoshimoto, T. IL-27 induces Th1 differentiation via p38 MAPK/T-bet- and intercellular adhesion molecule-1/LFA-1/ERK1/2-dependent pathways. *J. Immunol.* **177**, 7579–7587 (2006).
18. Cao, W. et al. p38 mitogen-activated protein kinase is the central regulator of cyclic AMP-dependent transcription of the brown fat uncoupling protein 1 gene. *Mol. Cell. Biol.* **24**, 3057–3067 (2004).
19. Cao, W., Medvedev, A. V., Daniel, K. W. & Collins, S. β-Adrenergic activation of p38 MAP kinase in adipocytes: cAMP induction of the uncoupling protein 1 (UCP1) gene requires p38 MAP kinase. *J. Biol. Chem.* **276**, 27077–27082 (2001).
20. Pirzgalska, R. M. et al. Sympathetic neuron-associated macrophages contribute to obesity by importing and metabolizing norepinephrine. *Nat. Med.* **23**, 1309–1318 (2017).
21. Imai, T. et al. Identification and molecular characterization of fractalkine receptor CX3CR1, which mediates both leukocyte migration and adhesion. *Cell* **91**, 521–530 (1997).

# Methods

### Mice

*Il27ra*-KO (B6N.129P2-*Il27ra*$^{tm1Mak}$/J, 018078), *Ebi3*-KO (B6.129X1-*Ebi3*$^{tm1Rsb}$/J, 008691), *Ucp1*-KO (B6.129-*Ucp1*$^{tm1Kz}$/J, 003124), *Cd2-cre* (B6.Cg-Tg(CD2-icre)4Kio/J, 008520), *Lyz2-cre* (B6.129P2-*Lyz2*$^{tm1(cre)Ifo}$/J, 004781), *Itgax-cre* (B6.Cg-Tg(Itgax-cre)1-1Reiz/J, 008068), *Cx3cr1-cre* (B6J.B6N(Cg)-*Cx3cr1*$^{tm1.1(cre)Jung}$/J, 025524), C57BL/6J (000664) and *Adipoq-cre* (B6.FVB-Tg(Adipoq-cre)1Evdr/J, 028020) mice were purchased from The Jackson Laboratory. *Ucp1-creERT2* mice[22] were from C. Wolfrum (ETH Zurich) provided by X. Yang (Yale University). *IL27ra*$^{flox/flox}$ (this paper) and *Il27p28*$^{flox/flox}$ mice[23] were generated in our laboratory. Animal experiments were performed according to ethical regulations and protocols approved by the Institutional Animal Care and Use Committee of Jinan University and the Institutional Animal Care and Use Committee of Yale University. All of the experiments used sex- and age-matched mice that were group-housed at four to six animals per cage. The animal studies in this work have been carried out on either sex and yield consistent results. Randomization was performed in all animal experiments. No statistical methods were used to predetermine the sample size. Mice were group housed in a temperature- and humidity-controlled, specific-pathogen-free animal facility at 25 °C under a 12 h–12 h light–dark cycle with free access to food and water. For the diet study, mice (aged 8 weeks) were fed a 60% HFD (Research Diets, D12492) for the indicated times. Mouse body weights were measured every week.

### Human samples

This study was approved by at the Institutional Review Board of the First Affiliated Hospital of Jinan University and was performed in accordance with the principle of the Helsinki Declaration II. Written informed consent was obtained from each participant. We recruited 42 individuals with obesity (BMI, 38.92 ± 1.349 kg m$^{-2}$, mean ± s.e.m., 42 for the Luminex immunoassay (Extended Data Fig. 1a) and 32 for intact IL-27 detection by ELISA (Fig. 1a and Extended Data Fig. 1b)), and 30 individuals with a healthy BMI (BMI, 20.69 ± 0.3144 kg m$^{-2}$, 26 for Luminex immunoassay (Extended Data Fig. 1a) and 30 for intact IL-27 detection by ELISA (Fig. 1a)). Information regarding the characteristics of the human cohorts is provided in Supplementary Table 1. Seven of the individuals with obesity (BMI between 37 and 51) underwent Roux En Y Gastric Bypass surgery. Information regarding the characteristics of each patient before and after surgery are provided in Supplementary Table 3. Bariatric procedures were performed laparoscopically by one single surgeon. The participants who had undergone Roux En Y Gastric Bypass surgery were evaluated by surgical dietitian treatment. We also recruited 12 individuals who had been diagnosed with type 2 diabetes (Supplementary Table 2). The exclusion criteria for recruitment were: hypertension; abdominal surgery; previous bariatric surgery; virus hepatitis; colitis; gastrointestinal disease and gastrointestinal surgery within 5 years before recruitment; and abnormal liver and kidney function. All of the participants were weighed in light clothing without shoes. Body height and weight were measured by a height–weight scale, and BMI (kg m$^{-2}$) was calculated.

### Reagents

The human serum samples were analysed on the Bio-Plex system (Bio-Rad) using a Bio-Plex Pro Human Cytokine 17-plex Assay (M5000031YV) and a Bio-Plex Pro Human Inflammation Panel 1 (171-AL001M). The Human IL-27 ELISA kit (434607) was purchased from BioLegend. Mouse serum samples were analysed by the Bio-Plex system using the 23-plex cytokine array kit (M60009RDPD). Glucose (63005518) was purchased from Sinopharm Chemical Reagent. Blood glucose strips (one-touch, accuracy to 0.1mg dl$^{-1}$) were purchased from Johnson & Johnson. Anti-p-AKT (S473) monoclonal antibodies (4060, D9E), anti-mouse AKT monoclonal antibodies (4685, 11E7), anti-GAPDH monoclonal antibodies (5174, D16H11), anti-HSP90 monoclonal antibodies (4877, C45G5), anti-PPARγ monoclonal antibodies (2435, C26H12), anti-mouse p-STAT3 (Y705) monoclonal antibodies (9145, D3A7), anti-STAT3 monoclonal antibodies (9139, 124H6), anti-p-p38 MAPK (T180/Y182) polyclonal antibodies (9211), anti-p38 MAPK polyclonal antibodies (9212), anti-p-STAT1 (Y701) monoclonal antibodies (9167, 58D6), anti-STAT1 monoclonal antibodies (14994, D1K9Y), anti-pATF2 (T71) polyclonal antibodies (9221) and anti-ATF2 monoclonal antibodies (35031, D4L2X) were purchased from Cell Signaling Technology. Anti-UCP1 polyclonal antibodies (ab10983), anti-mouse UCP1 monoclonal antibodies (ab209483, EPR20381), anti-PGC-1α polyclonal antibodies (ab54481), anti-PPARα polyclonal antibodies (ab24509), anti-mouse IL-27Rα monoclonal antibodies (ab220359, EPR20863-3, 110 kDa) and anti-IL-27Rα polyclonal antibodies (ab5997, 70 kDa) were purchased from Abcam. Anti-β-actin monoclonal antibodies (66009-1, 2D4H5) and anti-β-tubulin monoclonal antibodies (66240-1, 1D4A4) were purchased from Proteintech. APC/CY7-anti-mouse CD45 (557659, 30-F11), BV510-anti-mouse CD45.2 (740131, 104) and PE/CY7-anti-mouse CD11b (552850, M1/70) antibodies were purchased from BD Biosciences. PE-anti-mouse F4/80 (M100F1-09B, BM8), PE-anti-mouse CD8α (M10081-09B, 53.6.7), PE-anti-mouse IL-17 (M100I17-09B, 17F3) and APC-anti-mouse IFN-γ (M100I16-11A, XMG1.2) antibodies were purchased from Sungene Biotech. PerCP/CY5.5-anti-mouse CD4 (100434, GK1.5), FITC-anti-mouse CD19 (152404, 1D3/CD19), APC/CY7-anti-mouse CD45.1 (110716, A20), FITC-anti-mouse CD8α (100706, 53.6.7), BV421-anti-mouse IL-10 (505022, JES5-16E3), PE/CY7-anti-mouse CD3 (100220, 17A2) and Alexa Fluor 647-anti-mouse F4/80 (123122, BM8) antibodies were purchased from BioLegend. Recombined murine IL-27 (rmIL-27) (577408) was purchased from BioLegend. STAT3 inhibitors C188-9, stattic and HO-3867, and p38 MAPK inhibitors SB203580 and SB202190 were purchased from Selleck Chemicals. BODIPY TR Ceramide (D7540) was purchased from Invitrogen. The brown/beige adipose differentiation agents dexamethasone (D4902), rosiglitazone (R2408), indomethacin (I7378), isoproterenol (I5627), forskolin (F6886), 3-isobutyl-1-methylxanthine (I5879), triglyceride detection kit (T2449) and insulin (I3536) were purchased from Sigma-Aldrich. The leptin detection kit (MOB00B) and adiponectin detection kit (MRP300) were purchased from R&D, and the insulin detection kit (90080) was purchased from Crystal Chem.

### ELISA assays

Human serum was obtained as described above. Mouse serum was collected after feeding mice an HFD for 10 weeks. Assays using the ELISA kits for human IL-27 (434607, BioLegend), mouse leptin (MOB00B, R&D), mouse adiponectin (MRP300, R&D) and mouse insulin (90080, Crystal Chem) were performed according to the user manuals.

### Luminex immunoassay

Human serum was collected as mentioned above. The inflammatory factors in human serum were detected by Bio-Plex Pro Human Cytokine 17-plex Assay (M5000031YV) and a Bio-Plex Pro Human Inflammation Panel 1 (171-AL001M) using Bio-Plex 200 Multiplexing Analyzer System (Bio-Rad) as instructed by the user manuals. Mouse serum samples were analysed by the Bio-Plex system using the 23-plex cytokine array kit (M60009RDPD) as instructed by the user manuals.

### GTT

Mice were fasted for 12–18 h. Glucose (1 g kg$^{-1}$) was administered intraperitoneally (i.p.), and the blood glucose levels were measured at 0 min, 30 min, 60 min, 90 min and 120 min using blood glucose strips (Johnson & Johnson, accuracy to 0.1 mg dl$^{-1}$). The blood glucose level at 0 min was designated as the fasting glucose level.

### ITT

Mice were fasted for 2–4 h and i.p. injected with insulin (0.5 U kg$^{-1}$), blood glucose levels were measured at 0 min, 15 min, 30 min, 45 min,

60 min, 75 min, 90 min and 120 min using blood glucose strips. For the insulin sensitivity analysis, mice were fasted overnight, i.p. injected with insulin (0.75 U $kg^{-1}$), and epididymal fat was isolated at 15 min after injection and used for immunoblotting analysis.

### Triglyceride quantification

The concentration of triglycerides in the serum was quantified using a serum triglyceride determination kit (Sigma-Aldrich, Triglyceride Reagent, T2449, and Free Glycerol Reagent, F6428). For detection of triglycerides in the liver, 20–30 mg of tissue was homogenized in 500 µl of PBS and mixed with chloroform–methanol (2:1 (v/v)). The organic phase was transferred, air-dried overnight and resuspended in 1% Triton X-100 in absolute ethanol. The concentration of triglycerides was then quantified using the triglyceride determination kit.

### Serum biochemistry

Mice were fasted overnight. Whole blood was next collected, and serum cholesterol levels were determined using an automatic biochemistry analyser (7600-020, Hitachi).

### Western blot analysis

Whole-cell lysates or tissue lysates were extracted using RIPA lysis buffer (Beyotime) supplemented with complete protease inhibitor (Roche) and Phosphatase Inhibitor Cocktail 2 (P5726, Sigma-Aldrich), and the supernatants were used for the subsequent analysis. Proteins were diluted in loading dye (BL502A, Bio-sharp), heated at 95 °C for 10 min and run on 4–12% polyacrylamide gel. Proteins were transferred onto a polyvinylidene difluoride membrane and blotted with commercial antibodies mentioned in the figure legends and the 'Reagents' section. Each lane represents one biological independent sample in the immunoblot data. The band densities (grey values) for proteins of interest and housekeeping proteins were quantified using Image-Pro Plus v.6.0, the ratios of interested proteins and housekeeping proteins were calculated; for protein phosphorylation, the ratios of phosphorylated protein and total protein of interest were calculated, and the ratios were normalized and shown. The uncropped and unprocessed scans of immunoblot data are provided in Supplementary Fig. 1.

### Histology

Adipose, liver or the indicated tissues were fixed in 4% paraformaldehyde/1× PBS overnight at 4 °C and embedded in paraffin before sectioning. Sections were stained with H&E or Oil Red O (liver) and photographed under bright-field microscopy. A representative image for each group was shown in our study.

### Immunofluorescence

Cells were fixed in 4% paraformaldehyde for 10 min. After being blocked with 3% BSA/PBS, the cells were stained with an appropriate combination of primary antibodies, followed by staining with the corresponding fluorophore-conjugated secondary antibodies. The cells were mounted on coverslips and examined under a confocal microscope (Leica). Representative images for two independent experiments were shown in this work.

### Immunohistochemistry

The rabbit-Specific HRP/DAB (ABC) detection IHC Kit (ab64261, Abcam) was used for UCP1 immunohistochemistry according to the manufacturer's instructions. At least five biologically independent samples in each group were analysed and yielded similar results. A representative image for each group is shown.

### Cold challenge and core body temperature measurement

Cold-challenge experiments were performed within climate-controlled cold rooms. Mice were singly placed in individual precooled cages without bedding at 4 °C. Mice had free access to precooled food and water. Rectal core body temperatures were recorded every 2 h using a digital thermometer and rectal thermocouple probe (TH-212, HICHANCE). Individual mice were euthanized if their core body temperature fell below 20 °C, and scored as an event for the survival analysis.

### Metabolic cages

The energy consumption and energy expenditure of mice were measured using the Comprehensive Laboratory Animal Monitoring System (CLAMS, Columbus Instruments) metabolic cages housed within environment-controlled rodent incubators at Yale University. Mice were singly housed and acclimatized in metabolic chambers for 48 h before data collection. Mice had free access to food and water. Each mouse was continuously monitored for physical activity and food intake. $CO_2$ and $O_2$ levels were collected four times per hour per mouse over the duration of the experiment.

### RNA isolation and gene expression analysis

Total RNA was extracted from frozen tissue using TRNzol Universal Reagent (Tiangen) and quantified using a Nanodrop 2000 ultraviolet–visible spectrophotometer (Thermo Fisher Scientific). cDNA was prepared using 1 µg total RNA by a reverse transcription PCR using the PrimeScript RT Reagent Kit (TAKARA). Quantitative PCR was performed on cDNA using the TB Green Premix EX Taq II kit (TAKARA) with the CFX96 Real-Time PCR Detection System (Bio-Rad). Fold changes in expression were calculated with the $\triangle\triangle C_t$ method using mouse *HPRT* as the endogenous control. A list of primer pair sequences is provided in Supplementary Table 5.

### Bone marrow chimera

*Il27ra*-KO and WT mice (aged 10 weeks) were used as donor of bone marrow cells. Bone marrow was isolated from the femurs of hind legs. After red blood cell lysis and strained through cell strainer (40 µm), cell pellets were washed three times with sterile PBS, counted and stored on ice for later injection. Recipient *Il27ra*-KO and WT mice (aged 10 weeks) were lethally irradiated with 900 rads and transplanted with $1 \times 10^7$ bone marrow cells through ophthalmic vein injection. Mice were placed in specific-pathogen-free facilities supplemented with sterilized water and chow feed for 8 weeks to reconstitute the immune system and then processed for metabolism studies.

### Primary beige adipocytes preparation

Inguinal subcutaneous adipose tissue was minced and digested for 45 min at 37 °C in PBS containing collagenase II (1 mg $ml^{-1}$). Tissue suspension was filtered through a 100 µm cell strainer and centrifuged at 600*g* for 5 min to pellet the stromal vascular fraction (SVF). The pellet was further strained through 40 µm cell strainer and plated onto collagen-coated plates. After overnight incubation, the supernatant containing unadherent cells was removed. Preadipocytes were grown to confluence in DMEM with 10% FBS plus insulin (5 µg $ml^{-1}$). Confluent cells were induced to differentiate with dexamethasone (1 µM), 3-isobutyl-1-methylxanthine (0.5 mM), insulin (5 µg $ml^{-1}$), indomethacin (125 nM) and rosiglitazone (1 µM) for 2 d, followed by insulin (5 µg $ml^{-1}$) and triiodothyronine (1 nM) alone for another 5 d. The purity of cultured primary adipocytes was assessed by staining of CD45 followed by confocal microscopy. On day 7, cells were pretreated with and without IL-27 (100 ng $ml^{-1}$) for 12–24 h and then treated with isoproterenol (10 µM) or forskolin (10 µM) for 4–6 h. Cells were then lysed and used for immunoblotting analysis. For protein phosphorylation analysis, IL-27 (100 ng $ml^{-1}$) was added on day 7 for 0–120 min. For signalling inhibition experiments, STAT3 inhibitors (C188-9, 10 µM; stattic, 10 µM; or HO-3867, 20 µM) or p38 MAPK inhibitor (SB203580, 10 µM; or SB202190, 5 µM) were added into the culture medium 0.5 h before and during IL-27 treatment.

### Oxygen consumption measurements

Freshly isolated mouse inguinal SCW or BAT were rinsed with XF-DMEM (containing 25 mM HEPES) and cut into small pieces (~3 mg for BAT and ~4 mg for SCW). After extensive washing, one piece of tissue was placed in each well of a XF24 Islet Capture Microplate (Seahorse Bioscience) and covered with the islet capture screen that allows free perfusion while minimizing tissue movement. XF assay medium (500 µl) was added, and the samples were analysed in the XF24 Analyzer. These experiments were performed using 4–5 pieces per tissue per mouse, five individual mice per group. For SCW, the reagent concentrations were as follows: oligomycin (80 µM), FCCP (72 µM), and rotenone and antimycin A (240 µM and 120 µM, respectively). For BAT, the reagent concentrations were as follows: oligomycin (160 µM), FCCP (240 µM), and rotenone and antimycin A (480 µM and 360 µM, respectively).

### Flow cytometry analysis of immune cells

eWAT was minced and digested as described above. SVF pellets were used for surface staining of APC-CY7-anti mouse CD45, PE-Cy7-anti mouse CD11b and PE-anti mouse F4/80 antibodies. After incubation for 15 min, cells were washed with PBS and analysed using the BD FACSVerse Flow Cytometer (BD). The peripheral blood, inguinal lymph nodes, spleen, liver, BAT and SCW from bone marrow chimeric mice were collected and used for isolation of immune cells or SVF pellets. Cells were stained with APC-CY7-anti-mouse CD45.1, BV510-anti-mouse CD45.2, FITC-anti-mouse CD19, PerCP/CY5.5-anti-mouse CD4, PE-anti-mouse CD8α and Alexa Fluor 647-anti-mouse F4/80 antibodies. After incubation for 15 min, cells were washed with PBS and analysed using the BD FACSVerse Flow Cytometer (BD). FACS data were analysed using FlowJo v.10. The gating strategies are provided in Supplementary Fig. 2.

### Generation of IL-27Rα conditional KO mice

The generation of *Il27ra*$^{flox/flox}$ mice was performed by the Cyagen Biotechnology using gene-targeting technology. In brief, a 997 bp conditional KO region containing exon 3 and exon 4 of *IL27ra* gene (GenBank: NM_016671.3), a 5.2 kb 5′ homology arm and a 3 kb 3′ homology arm were amplified from a bacterial artificial chromosome clone using high fidelity Taq, and were sequentially assembled into a targeting vector together with recombination sites and a neomycin selection cassette. The final targeting vector was confirmed by digestion with multiple restriction enzymes and full sequencing, then transformed into C57BL/6 mice embryonic stem cells by electroporation. Correct embryonic stem cell clones were identified and injected into C57BL/6 mouse blastocysts. Chimaera mice were visibly identified and crossed with Flp-deleter to delete the neomycin selection cassette. The germ line transmission was confirmed by genotyping PCR. The offspring with the *Il27ra*$^{flox/WT}$ genotype were then crossed with *Cd2-cre*, *Lyz2-cre*, *Adipoq-cre* or *Ucp1-creERT2* mice. The mice with the expected genotype were used for experiment. The genotyping primers to detect the flox (331 bp) or WT (257 bp) band were as follows: forward: 5′-CTGGTTCTGGTATGGTTTGGGGTT-3′, reverse: 5′-TGAA AGAACTCAACAGTGGGCCGG-3′.

### IL-27 administration

WT, *Il27ra*$^{flox/flox}$, *Adipoq-cre*;*Il27ra*$^{flox/flox}$, *Ucp1-creERT2*;*Il27ra*$^{flox/flox}$ or *Ucp1*-KO mice (aged 8 weeks) were fed an HFD for 12–32 weeks to induce severe obesity. *Ucp1-creERT2*;*Il27ra*$^{flox/flox}$ mice were pretreated with tamoxifen before IL-27 therapy (see below). Mice of each genotype were randomly divided into two groups for i.p. injection of rmIL-27 (100 µg kg$^{-1}$) or PBS every other day for 15 d, and then processed for metabolic analysis. *Ebi3*-KO mice (aged 12 months) were randomly divided into two groups and i.p. injected with rmIL-27 (100 µg kg$^{-1}$) or PBS every day for 7 d, and then placed at 4 °C for cold-challenge experiments.

### Tamoxifen preparation and treatment

Tamoxifen (Sigma-Aldrich, T5468) was dissolved in sunflower seed oil/ethanol (9:1 v/v) at 20 mg ml$^{-1}$ by shaking at 37 °C for 15 min. Mice (aged 8–10 weeks) were i.p. injected with 2 mg per mouse four times over a period of 7 d. After another 7 d, mice were subjected to HFD feeding, cold stimulation or IL-27 administration for the indicated time.

### RNA sequencing

Total RNA was extracted using the mirVana miRNA Isolation Kit (Ambion) according to the manufacturer's protocol. RNA integrity was evaluated using the Agilent 2100 Bioanalyzer (Agilent Technologies). The samples with an RNA integrity number of ≥7 were processed for the subsequent analysis. The transcriptome sequencing and analysis were conducted by OE biotech. Raw data (raw reads) were processed using Trimmomatic. The reads containing ploy-N and the low-quality reads were removed to obtain the clean reads. The clean reads were next mapped to the reference genome using hisat2. Fragments per kb of transcript per million mapped reads and read count values of each transcript (protein_coding) was calculated using bowtie2 and eXpress. Differentially expressed genes (DEGs) were identified using the DESeq (2012) functions estimatSizeFactors and nbinomTest. $P < 0.05$ and a fold change of >2 or <0.5 was set as the threshold for a significant differential expression pattern. Hierarchical cluster analysis of DEGs was performed to examine transcript expression patterns. Gene Ontology enrichment analysis and KEGG pathway enrichment analysis of DEGs were performed using R based on the hypergeometric distribution.

### Statistics and reproducibility

All the non-human experiments and data shown in this work have been repeated at least twice with consistent results. The presented data were performed on biologically independent samples. GraphPad Prism (v.8) was used for graphing and statistical analysis. All statistical tests are fully described in the figure legends and met the criteria for normal distribution with similar variance. No statistical methods were used to predetermine sample sizes. Two tailed student's *t*-tests were used for comparisons between two groups. For assessment between more than two groups, one-way ANOVA was used. For assessment between two independent variables, two-way ANOVA was used; Sidak's multiple comparisons test was also performed when comparing the difference at each time point. For survival analysis, a log-rank test was performed. For correlation analysis, linear regression analysis was performed. Data are presented as mean (average) ± s.e.m. unless otherwise stated. $P < 0.05$ was considered to be statistically significant and the exact *P* values are provided in the figures.

### Reporting summary

Further information on research design is available in the Nature Research Reporting Summary linked to this paper.

## Data availability

Our RNA-seq data are available at the Sequence Read Archive (SRA) repository at NCBI under the accession numbers SRX10969398–SRX10969403. Source data are provided with this paper.


22. Rosenwald, M., Perdikari, A., Rulicke, T. & Wolfrum, C. Bi-directional interconversion of brite and white adipocytes. *Nat. Cell Biol.* **15**, 659–667 (2013).
23. Zhang, S. et al. High susceptibility to liver injury in IL-27 p28 conditional knockout mice involves intrinsic interferon-gamma dysregulation of CD4$^+$ T cells. *Hepatology* **57**, 1620–1631 (2013).



**Acknowledgements** We thank A. Xu from Hongkong University, L. Ye from the Third Military Medical University, B. Li from Shanghai Jiao Tong University, Y. Qiu from Peking University, Y. Huo from Guangzhou Medical University and J. Chen from Sun Yat-Sen University for discussion, comments and technical guidance; and C. Cote for English language editing of this manuscript. This work is supported by the National Key Research and Development

Program of China (no. 2020YFA0803502 to Z.Y.; no. 2017YFA0205200 to L.L.), the National Natural Science Foundation of China (nos 31830021, 32030036 and 31420103901 to Z.Y.; no. 81771957 to L.L.; no. 32070121 to H.Y.; no. 31800721 to Q. Wang; and no. 31500742 to Q.S.), the 111 Project (no. B16021 to Z.Y.), the Incubating Program from the Science and Technology Department of Guangdong Province of China (no. 2014A030308003 to Z.Y.), China Postdoctoral Science Foundation (nos 2018M633278 and 2020M683159 to Q. Wang; no. 2020M673045 to H.Z.).

**Author contributions** Q. Wang, D.L., G.C. and Q.S. conceived this research. Q. Wang, D.L., J.Z., M.Z., H.C. and Q. Wen performed experiments and analysed data. Q.S., C.W. and C.Y. analysed the human samples. H.X. helped with HFD treatment. L. Zhu, H.Z., B.W. and G.L. facilitated in western blot experiments. R.J.P. carried out the metabolic cage experiments and O.S. assisted with cold challenge experiments. Y.Y., S.H. and Y.C. provided technical support for primary adipocyte culture. Z.L. helped in ordering reagents. X.W., Q.Z., Z.J., H.L. and Y.X. assisted in the revision of the manuscript. L. Zhou provided the cold room. C.W. carried out the gastric bypass surgery. X.Y., Y.L., G.I.S. and V.D.D. helped in conceiving the project and afforded guidance in discussions. Q. Wang, G.C. and Z.Y. wrote the manuscript with help from D.L., Q.S., J.Z. and M.Z. L.L., H.Y., R.A.F. and Z.Y. helped in conceiving the project, mentored and supervised its participants.

**Competing interests** Z.Y., Q. Wang and H.Y. have applied a patent with China National Intellectual Property Administration, with Jinan University as the applicant, Z.Y., Q. Wang and H.Y. as the inventors. The application number is 202110986914.X, and the patent covers the screening of IL-27Rα agonists for promoting UCP1 production. The other authors (D.L., G.C., Q.S., J.Z., M.Z., H.C., Q. Wen, H.X., L. Zhu, H.Z., R.J.P., O.S., Y.Y., S.H., Y.C., B.W., G.L., Z.L., C.Y., X.W., L. Zhou, Q.Z., Z.J., H.L., Y.X., X.Y., C.W., Y.L., G.I.S., V.D.D., L.L. and R.A.F.) declare no competing interests.

**Additional information**

**Supplementary information** The online version contains supplementary material available at https://doi.org/10.1038/s41586-021-04127-5.

**Correspondence and requests for materials** should be addressed to Ligong Lu, Hengwen Yang, Richard A. Flavell or Zhinan Yin.

**Peer review information** *Nature* thanks the anonymous reviewers for their contribution to the peer review of this paper.

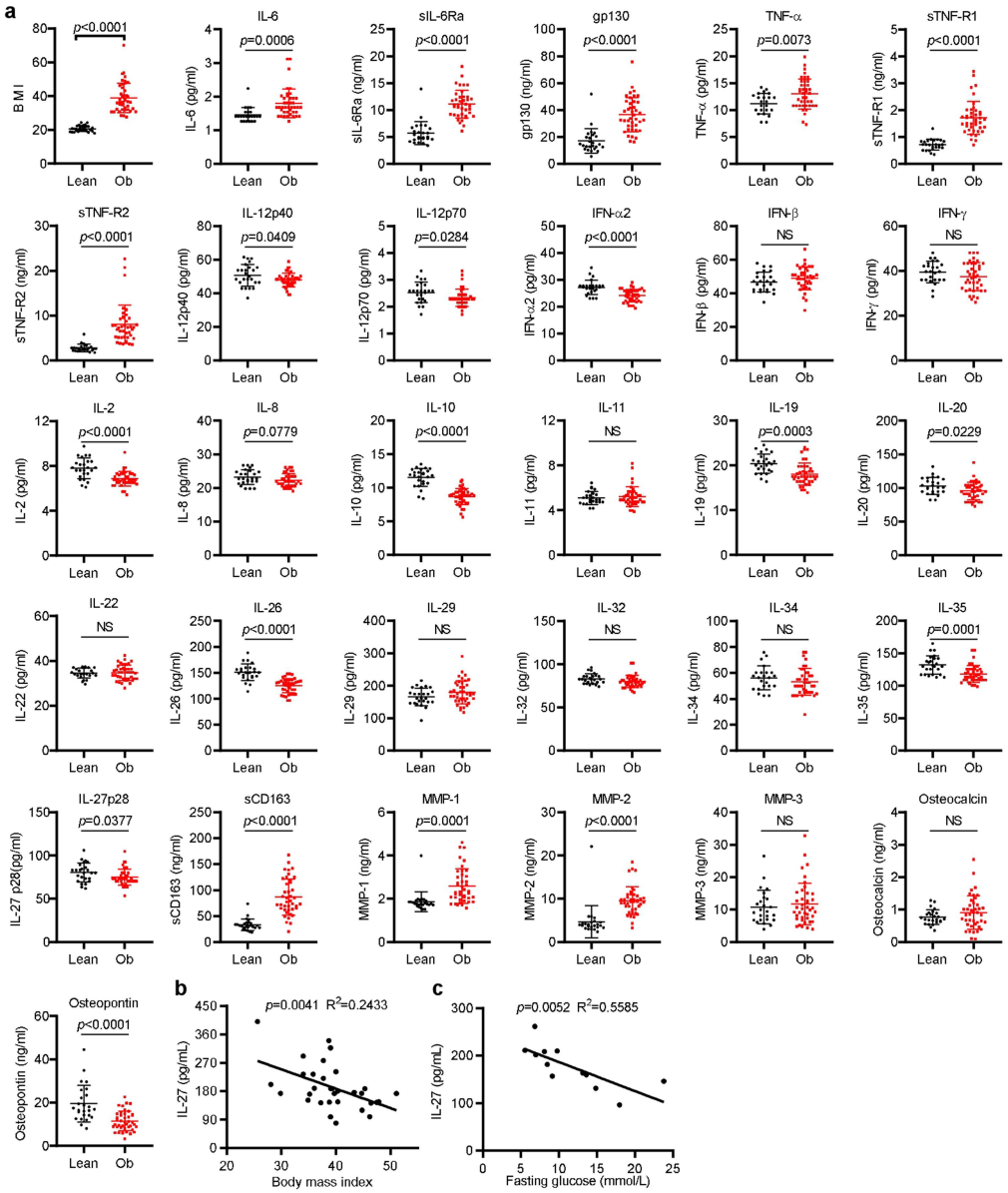


**Extended Data Fig. 1 | Reduced serum IL-27 level in obese subjects.** **a**. Serum from obese human subjects (n = 42) and lean healthy controls (n = 26) were used for detection of inflammatory factors by Bio-Rad Bio-Plex 200 Multiplexing Analyzer System. The body mass index (BMI) of individual subject was presented in the first panel. **b**. Serum IL-27 level in obese patients was detected by ELISA as in Figure 1a. Correlation of BMI and serum IL-27 level in obese subjects was analysed and shown (n = 32). **c**. Correlation of fasting glucose and serum IL-27 level in type 2 diabetes (T2D) patients (n = 12). Data are mean ± s.d. of biologically independent samples. Two-tailed unpaired student's *t*-test (**a**); linear regression analysis (**b** & **c**). NS, not significant.

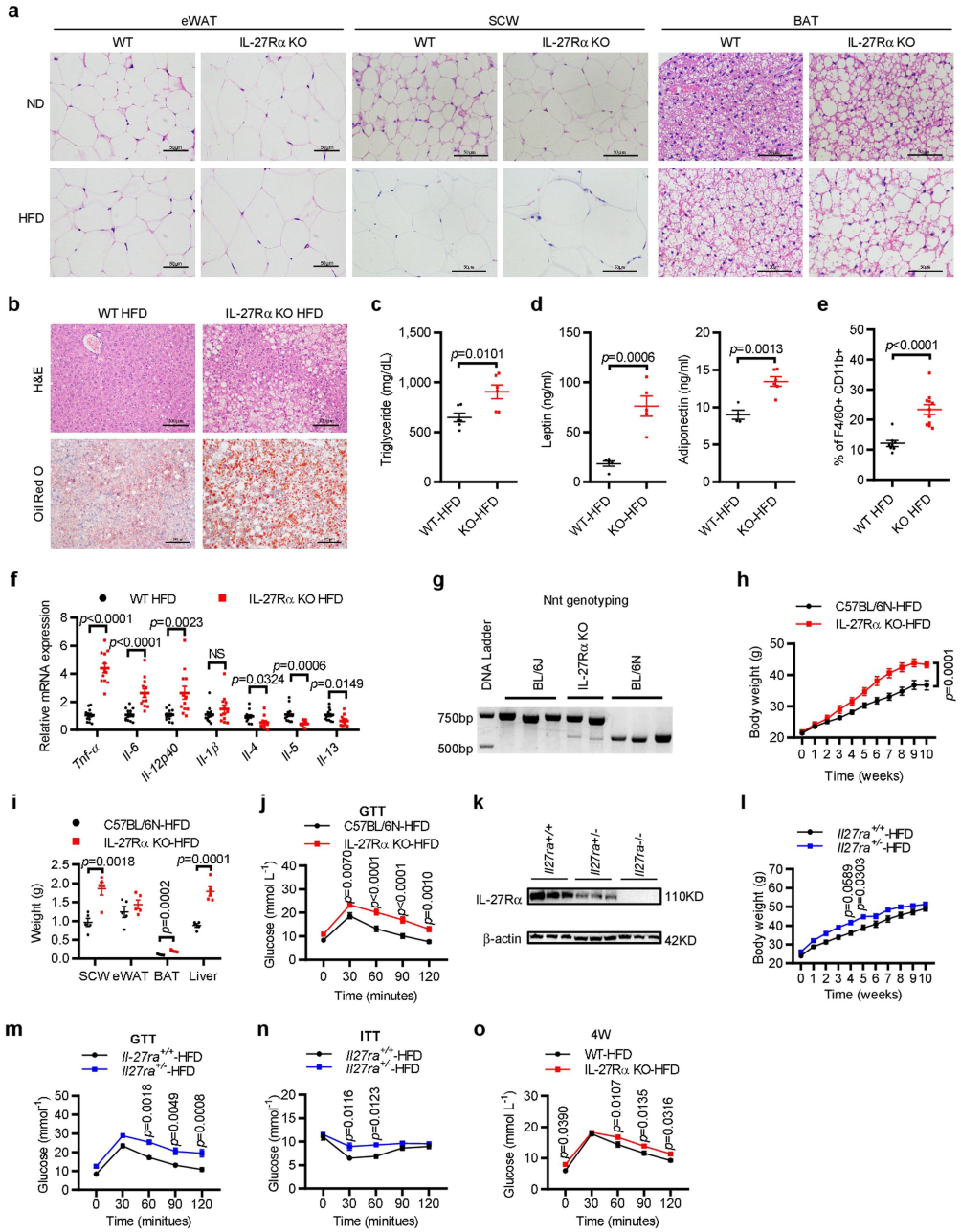


**Extended Data Fig. 2 | IL-27Rα deficiency aggravates HFD-induced obesity.** IL-27Rα KO and WT mice at 8 weeks of age were fed on HFD or ND for 10 weeks (**a**–**f**). **a**. Histology (H&E) slides of epididymal white adipose tissue (eWAT), subcutaneous white adipose tissue (SCW) and brown adipose tissue (BAT). Scale bar = 50μm. **b**. Histology (H&E) and oil red O staining of liver from HFD treated mice. Scale bar = 100μm. Serum was collected after 10 weeks HFD treatment and triglyceride (**c**, n=6), (**d**) leptin (n = 5) and adiponectin (n = 4 for WT and n = 6 for KO) were detected. **e**. The infiltrated macrophages in the stromal vascular fraction (SVF) of epididymal fat were analysed by FACS, the statistical analysis of macrophage percentage in CD45+ is shown (n = 8 for WT and n = 11 for KO). **f**. Realtime PCR analysis of key cytokines in epididymal fat (eWAT) from mice fed on HFD for 10 weeks (n = 12 for WT-*Il4* and n = 10 for KO-*Il4*, n = 13-WT and n = 12-KO for the rest genes). **g**. C57BL/6J, IL-27Rα KO and C57BL/6N mice were genotyped via *Nnt* gene PCR. **h**–**j**. IL-27Rα KO and C57BL/6N mice at 8 weeks of age were fed on HFD for 10 weeks. **h**. Body weight was recorded each week (n = 14 for C57BL/6N and n = 10 for KO). **i**. Adipose tissues and livers were collected and weighted (n=5). **j**. GTT was performed (n = 14 for C57BL/6N and n = 10 for KO). **k**. The splenocytes were isolated from *Il27ra*+/+, *Il27ra*+/- and *Il27ra*-/- mice and protein samples were used for immunoblotting analysis of IL-27Rα. Each lane represents one biological independent sample. **l**–**n**. *Il27ra*+/- and *Il27ra*+/+ mice at 8 weeks of age were fed on HFD for 10 weeks. **l**. Body weight was recorded each week (n = 10 for *Il27ra*+/+ and n = 5 for *Il27ra*+/-). GTT (**m**, n = 3 for *Il27ra*+/+ and n = 6 for *Il27ra*+/-) and ITT (**n**, n = 4 for *Il27ra*+/+ and n = 7 for *Il27ra*+/-) were performed. **o**. IL-27Rα KO (n = 18) and WT (n = 12) mice at 8 weeks of age were fed on HFD, GTT was performed after 4 weeks of HFD treatment. All experiments were repeated at least twice with similar results. Data are mean ± s.e.m. of biologically independent samples. Two-tailed unpaired student's test (**c**–**f** & **i**); two-way ANOVA (**h**); two-way ANOVA with Sidak's multiple comparisons test (**j** & **l**–**o**). NS, not significant.

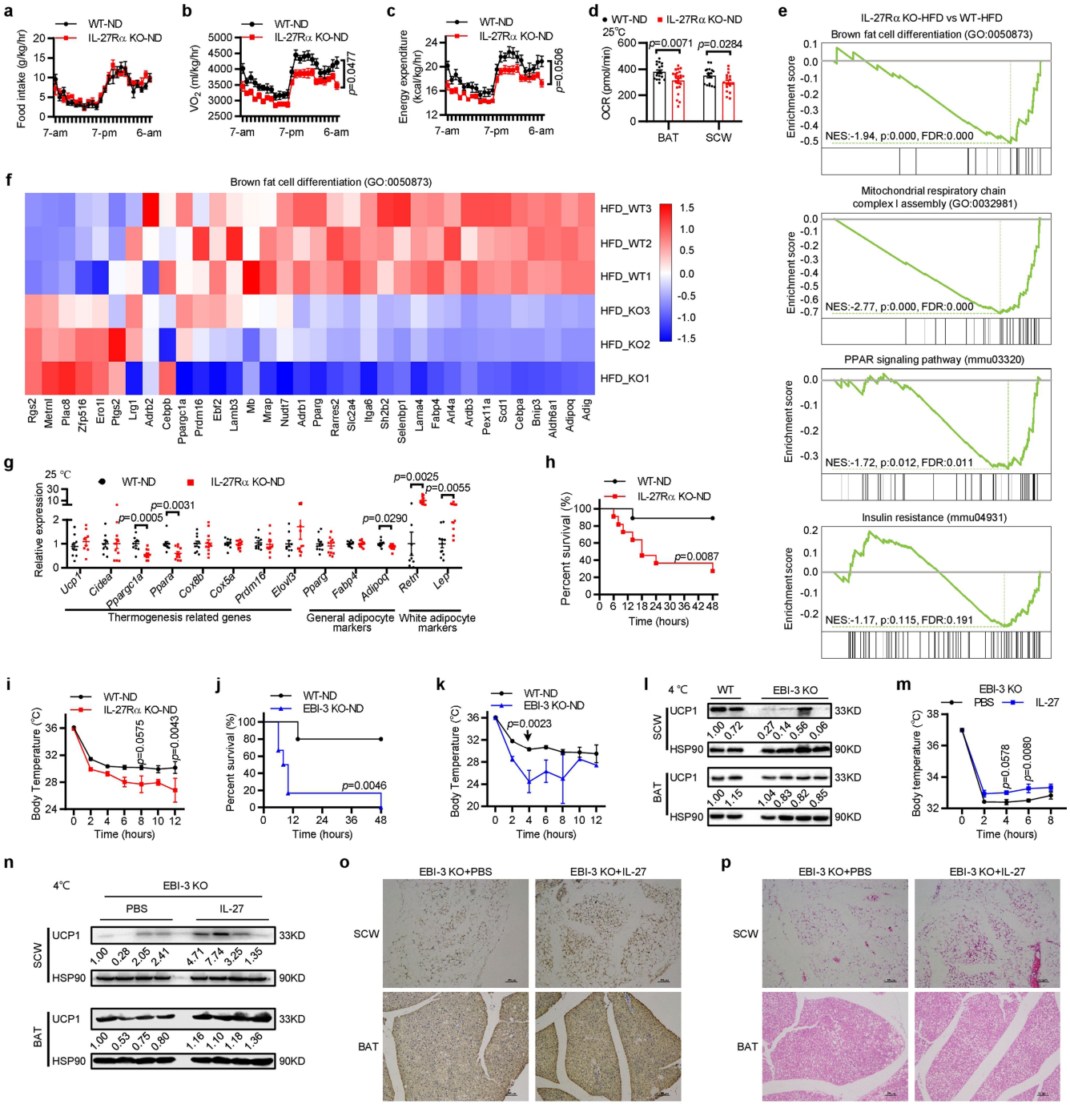


**Extended Data Fig. 3** | See next page for caption.

**Extended Data Fig. 3 | Reduced energy expenditure and thermogenesis in IL-27 signalling deficient mice. a**–**c**. IL-27Rα KO and WT mice at 8 weeks of age were placed in metabolic cages. The food intake (**a**, n = 8 for WT and n = 7 for KO), oxgen consumption (**b**, n = 8) and energy expenditure (**c**, n = 8) were shown. **d**. BAT and SCW tissues were isolated from WT-ND and IL-27Rα KO-ND mice at 6-8 weeks of age, cut into small pieces (~0.003g for BAT and ~0.004g for SCW) and used for detection of basal oxygen consumption rate by Seahorse XF Analyzer (n = 5 mice per group, 18 pieces for WT-BAT, 23 pieces for KO-BAT and 17 pieces for SCW samples). **e** & **f**. IL-27Rα KO and WT mice at 8 weeks of age were fed on HFD for 10 weeks, SCW were collected for RNA-seq analysis. **e**. Gene set enrichment analysis was performed for indicated pathways. Genes were ranked according to their expression. NES, normalized enrichment score; FDR, false discovery rate. **f**. Heat maps of differentially expressed genes in indicated pathway. **g**. Gene expression in SCW from IL-27Rα KO and WT mice on normal diet were determined by real-time PCR (n = 9 for WT-*Ucp1*, WT-*Cidea*, WT-*Adipoq* and WT-*Retn*, n = 10 for WT-*Ppargc1a*, WT-*Ppara*, WT-*Cox8b*, WT-*Cox5a*, WT-*Prdm16* and WT-*Elovl3*, n = 11 for WT-*Pparg*, WT-*Fabp4* and WT-*Lep*, n = 8 for KO-*Ucp1*, n = 10 for KO-*Retn*, n=11 for the rest KO mRNAs). **h**. Survival curve of IL-27Rα KO and WT mice fed on ND in response to cold challenge (4 °C, n = 9 for WT and n=11 for KO). **i**. Rectal temperature of mice fed on ND in response to cold challenge (4 °C, n = 9 for WT and n = 11 for KO). **j**–**l**. EBI-3 KO mice and WT controls fed on normal chow were challenged at 4 °C. The survival curve (**j**) and rectal temperature (**k**) were recorded and shown (n = 5 for WT and n=6 for KO). After 12 hours of cold stimulation, BAT and SCW were collected, lysed and used for immunoblotting analysis of UCP1 (**l**). **m**-**p**. EBI-3 KO mice were i.p. injected with rmIL-27 (100μg/kg) or PBS every day for 7 days and then challenged at 4°C. **m**. Rectal temperature of mice in response to cold was shown (n = 6). **n**. Immunoblot analysis of protein extracts from SCW and BAT after 24 hours of cold challenge. UCP1 staining (**o**) and histology analysis (**p**) (Scale bar = 100μm). Representative sections were shown. (**l** & **n**) Each lane represents one biological independent sample and band densities were quantified with ImageJ, ratios of UCP1/HSP90 were normalized. All experiments were repeated at least twice with similar results. Data are mean ± s.e.m. Data represent biologically independent samples except for **d**. Two-tailed unpaired student's t-test (**d** & **g**); two-way ANOVA (**a**–**c**); two-way ANOVA with Sidak's multiple comparisons test (**i**, **k** & **m**); log-rank test (**h** & **j**); Gene Set Enrichment Analysis (**e**).

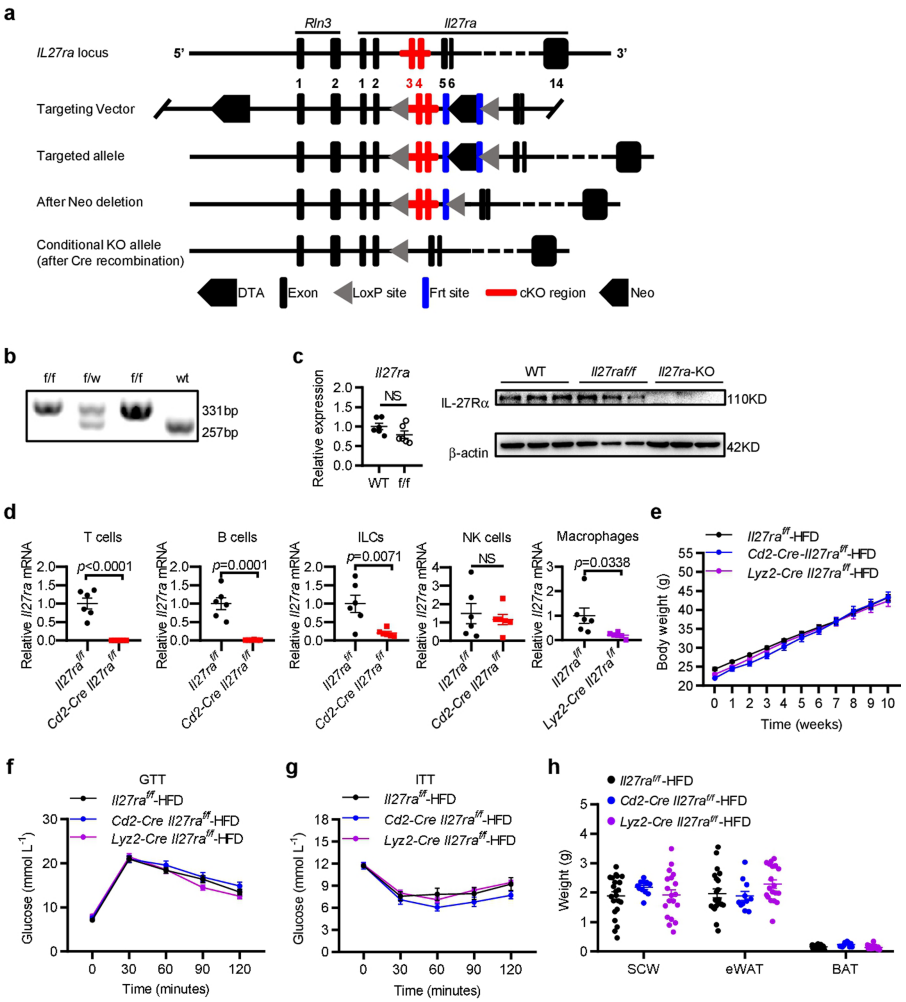


**Extended Data Fig. 4 | The counteracting obesity effects of IL-27Ra signalling was not through direct actions on CD2+ lymphoid or Lyz2+ myeloid cells. a**. Schematic model for the generation of *Il27ra*$^{flox/flox}$ mice. The *Il27ra* locus (top) was targeted by the targeting vector (second), which contains the homologous sequence of *Il27ra*, including two LoxP sites flanking exons 3&4, and a Neo selecting cassette. The linearized vector was subsequently delivered to embryonic stem cells (C57BL/6) via electroporation, followed by drug selection, PCR screening, and Southern Blot confirmation. Homologous recombination resulted in the floxed allele (Third). After confirming correctly targeted ES clones via Southern Blotting, selected clones were used for blastocyst microinjection to produce the F0 generation. The F1 were confirmed as germline-transmitted via crossbreeding F0 with Flp-deleter to delete Neo cassette (Fourth). After Cre recombination, the floxed *Il27ra* allele will results in the deletion of exons 3 and 4 (bottom). **b**. Genotyping of *Il27ra*$^{f/f}$ mice. **c**. IL-27Rα expression in spleen from *Il27ra*$^{f/f}$ and WT mice were determined by Real-time PCR (n = 6, left) and Western Blot (right, each lane represents one biological independent sample). **d**. *Il27ra* gene expression in FACS sorted CD3+ T cells, CD45+ CD19+ B cells, CD45+ Lin- (CD3- CD4- CD8a- CD19- CD11b- Ly6c-) CD90.2+ CD127+ ILCs, CD45+ CD3- NK1.1+ NK cells from the spleen of *Il27ra*$^{f/f}$ and *Cd2-Cre Il27ra*$^{f/f}$ mice were determined by Real-time PCR (n = 6, left 4 panels). Thioglycollate was intraperitoneally injected into *Il27ra*$^{f/f}$ and *Lyz2-Cre Il27ra*$^{f/f}$ mice for 4 days, and then the peritoneal macrophages were collected for the detection of *Il27ra* gene expression by Real-time PCR (n = 6, last panel). **e-h**. *Il27ra*$^{f/f}$, *Cd2-Cre Il27ra*$^{f/f}$ and *Lyz2-Cre Il27ra*$^{f/f}$ mice at 8 weeks of age were fed on HFD for 10 weeks. **e**. Body weight was recorded each week (n = 21 for *Il27ra*$^{f/f}$, n=11 for *Cd2-Cre Il27ra*$^{f/f}$ and n = 18 for *Lyz2-Cre Il27ra*$^{f/f}$). GTT (**f**, n = 15 for *Il27ra*$^{f/f}$, n = 11 for *Cd2-Cre Il27ra*$^{f/f}$ and n = 19 for *Lyz2-Cre Il27ra*$^{f/f}$) and ITT (**g**, n = 13 for *Il27ra*$^{f/f}$, n = 12 for *Cd2-Cre Il27ra*$^{f/f}$ and n = 19 for *Lyz2-Cre Il27ra*$^{f/f}$) were performed after 10 weeks of HFD treatment. **h**. Adipose tissues were collected and weighted after 10 weeks of HFD treatment (n = 22 for *Il27ra*$^{f/f}$, n = 11 for *Cd2-Cre Il27ra*$^{f/f}$ and n = 19 for *Lyz2-Cre Il27ra*$^{f/f}$). All experiments were repeated at least twice with similar results. Data are mean ± s.e.m. of biologically independent samples. Two-tailed unpaired student's test (**c**, **d**); two-way ANOVA (**e**–**g**); one-way ANOVA (**h**). NS, not significant.

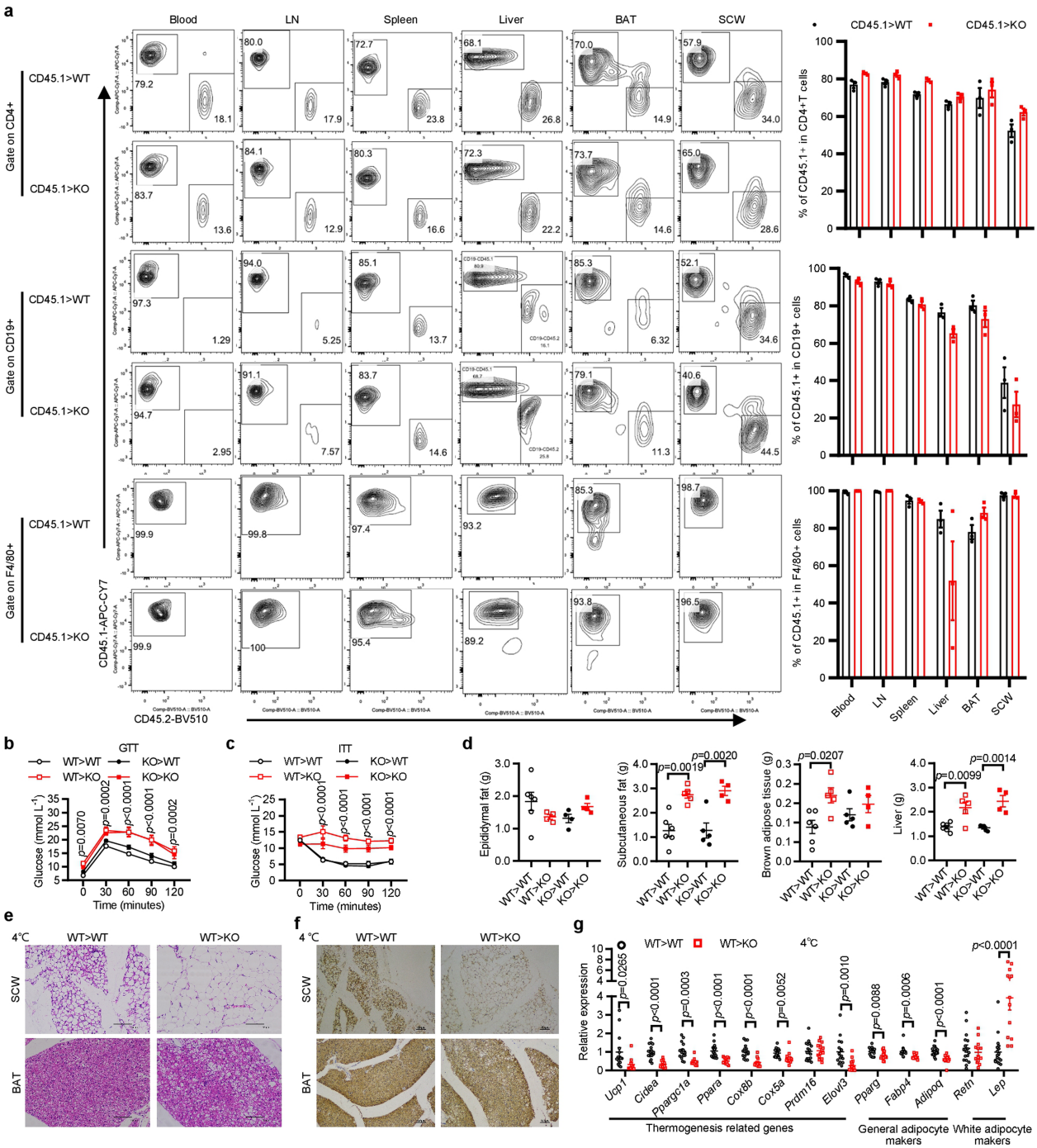


**Extended Data Fig. 5 | The phenotypes of IL-27Rα KO and WT chimeras in HFD-induced obesity and adaptive thermogenesis. a**. Bone marrow cells from CD45.1 WT strain were transferred into irradiated CD45.2 IL-27Rα KO or CD45.2 WT hosts (1 x $10^7$cells/mouse) to generate chimera. Mice were housed for 8 weeks to reconstitute the immune system. Immune cells were isolated from different tissues as indicated, the percentages of donor (CD45.1+) and host (CD45.2+) cells in CD4+ T (top), CD19+ B (middle) or F4/80+ macrophages (bottom) were analysed via FACS (n = 3). **b**–**d**. Bone marrow chimeras were generated as in Fig. 3a and fed on HFD. GTT (**b**, n = 13 for WT>WT, n = 11 for WT>KO, n = 12 for KO>WT and n = 10 for KO>KO) and ITT (**c**, n = 5 for WT>WT, n = 7 for WT>KO, n = 6 for KO>WT and n = 6 for KO>KO) were performed after 10 weeks of HFD treatment. **d**. Epididymal adipose (n = 6 for WT>WT, n = 4 for the rest groups), subcutaneous adipose, brown adipose tissue and liver (n = 6 for WT>WT, n = 5 for WT>KO, n = 5 for KO>WT and n = 4 for KO>KO) were collected and weighted after 10 weeks of HFD treatment. **e**–**g**. Chimeric mice fed on normal chow were challenged at 4 °C for 12 hours, SCW and BAT were collected for histology analysis (**e**, H&E, scale bar = 100μm) or immunohistochemical staining of UCP1 (**f**, scale bar = 100μm). Real-time PCR analysis of gene expression in SCW was also performed and shown (**g**, in WT>WT group, n = 15 for *Ucp1*, n=16 for *Cidea*, *Ppargc1a* and *Elovl3*, n = 17 for *Cox8b* and *Retn*, n=18 for the rest genes; in WT>KO group, n = 11 for *Ucp1*, n = 12 for *Cidea*, *Ppargc1a*, *Ppara* and *Lep*, n=13 for *Cox8b*, *Prdm16* and *Retn*, n = 14 for *Cox5a* and *Fabp4*, n = 15 for *Elovl3*, *Pparg* and *Adipoq*). All experiments were repeated at least twice with similar results. Data are mean ± s.e.m. of biologically independent samples. Two-tailed unpaired student's t-test (**a** & **g**); one-way ANOVA (**d**); two-way ANOVA with Sidak's multiple comparisons test (**b** & **c**).

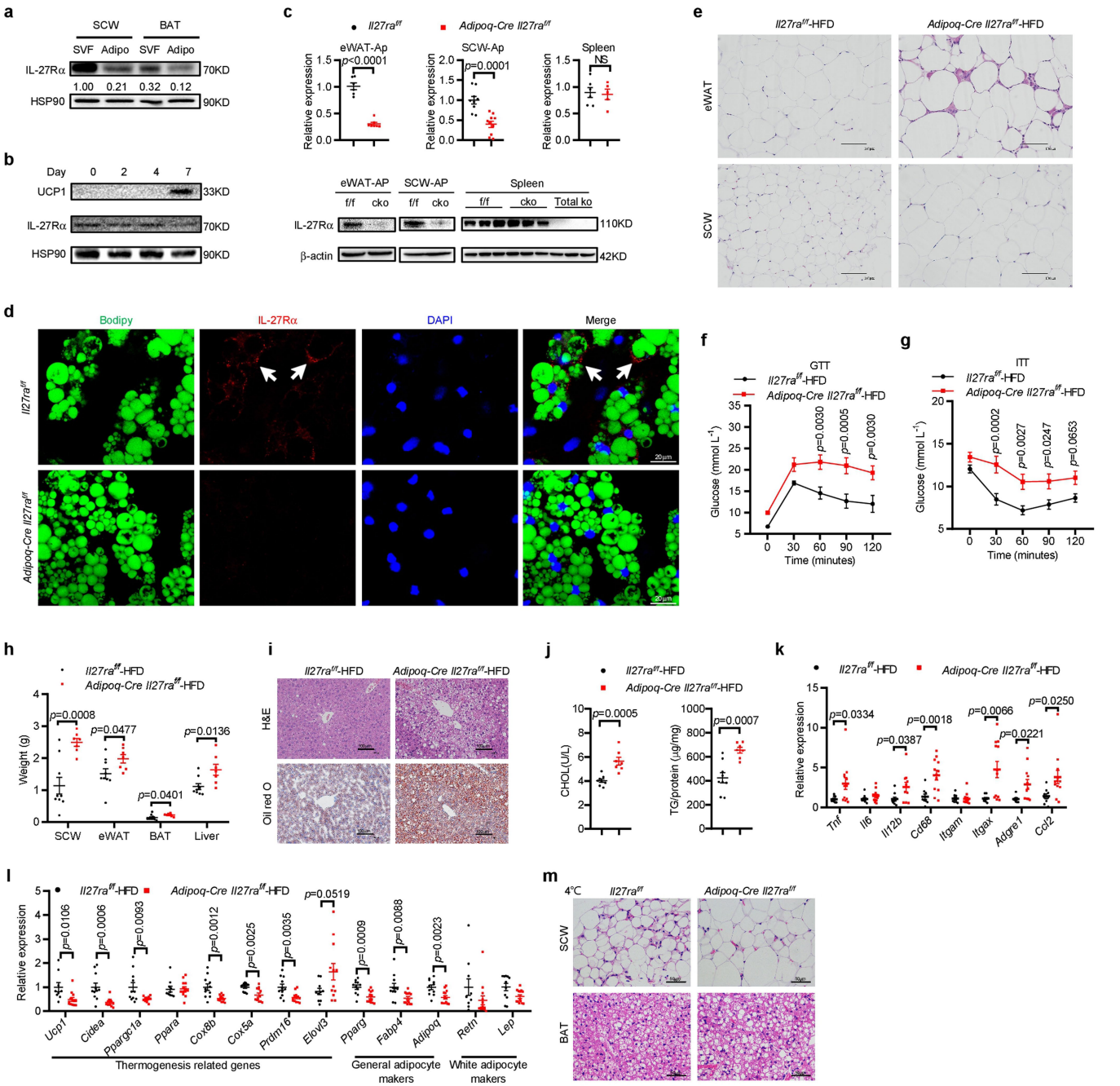


**Extended Data Fig. 6 | *Adipoq-Cre Il27ra$^{f/f}$* mice were hypersensitive to HFD-induced obesity. a.** Immunoblot analysis of IL-27Rα expression in stromal vascular fraction (SVF) and adipocyte fraction of SCW and BAT from WT mice. **b.** Immunoblot analysis of IL-27Rα during the primary beige adipocyte differentiation from SVF of WT SCW. **c.** IL-27Rα expression in adipocyte fraction of eWAT / SCW or spleen from *Il27ra$^{f/f}$* and *Adipoq-Cre Il27ra$^{f/f}$* mice were determined by Real-time PCR (above; for *Il27ra$^{f/f}$* samples, n=6 for eWAT and spleen, n = 9 for SCW; for *Adipoq-Cre Il27ra$^{f/f}$* samples, n = 7 for eWAT, n = 10 for SCW and n = 5 for spleen) and Western Blot (below). **d.** Primary adipocytes were differentiated *in vitro* from SCW of *Il27ra$^{f/f}$* and *Adipoq-Cre Il27ra$^{f/f}$* mice. IL-27Rα protein expression was detected by immunofluorescence. IL-27Rα (Red), lipid droplet (Bodipy, Green) and cell nucleus (DAPI, Blue), scale bar = 20μm. **e**–**l.** *Adipoq-Cre Il27ra$^{f/f}$* mice and *Il27ra$^{f/f}$* controls at 8 weeks of age were fed on HFD for 10 weeks. **e.** Histology (H&E) staining of epididymal and subcutaneous fat tissue from HFD treated mice. Scale bar=100μm. GTT (**f**, n = 9 for *Il27ra$^{f/f}$* and n = 7 for *Adipoq-Cre Il27ra$^{f/f}$*), ITT (**g**, n=19 for *Il27ra$^{f/f}$* and n=14 for *Adipoq-Cre Il27ra$^{f/f}$*) and the weight of indicated tissues (**h**, n = 9 for *Il27ra$^{f/f}$* and n = 7 for *Adipoq-Cre Il27ra$^{f/f}$*) were detected after 10 weeks of HFD treatment. **i.** Histology (H&E) and oil red O staining of liver from HFD treated mice. Scale bar = 100μm. **j.** Serum cholesterol (CHOL, n = 8 for *Il27ra$^{f/f}$* and n = 7 for *Adipoq-Cre Il27ra$^{f/f}$*) and liver triglyceride (TG, n=9 for *Il27ra$^{f/f}$* and n=7 for *Adipoq-Cre Il27ra$^{f/f}$*) were detected. **k.** Realtime PCR analysis of inflammatory genes expression in eWAT (n = 9 for *Il27ra$^{f/f}$* samples, for *Adipoq-Cre Il27ra$^{f/f}$* group, n = 10 for *Il12b*, n=13 for *Il6* and n = 12 for the rest genes). **l.** Realtime PCR analysis of adipose related genes expression in SCW of mice housed at room temperature (for *Il27ra$^{f/f}$* samples, n = 9 for *Ucp1*, n = 10 for *Ppara*, *Elovl3* and *Retn*, n=12 for *Cox5a* and n = 11 for the rest genes; for *Adipoq-Cre Il27ra$^{f/f}$* group, n = 12 for *Cox5a* and *Elovl3*, n = 13 for the rest genes). **m.** *Adipoq-Cre Il27ra$^{f/f}$* and *Il27ra$^{f/f}$* mice fed on normal chow were challenged at 4 °C for 12 hours, SCW and BAT were collected for histology analysis (H&E). Scale bar = 50μm. All experiments were repeated at least twice with similar results. Data are mean ± s.e.m. of biologically independent samples. Two-tailed unpaired student's t-test (**c**, **h**, **j**–**l**); two-way ANOVA with Sidak's multiple comparisons test (**f** & **g**). NS, not significant.

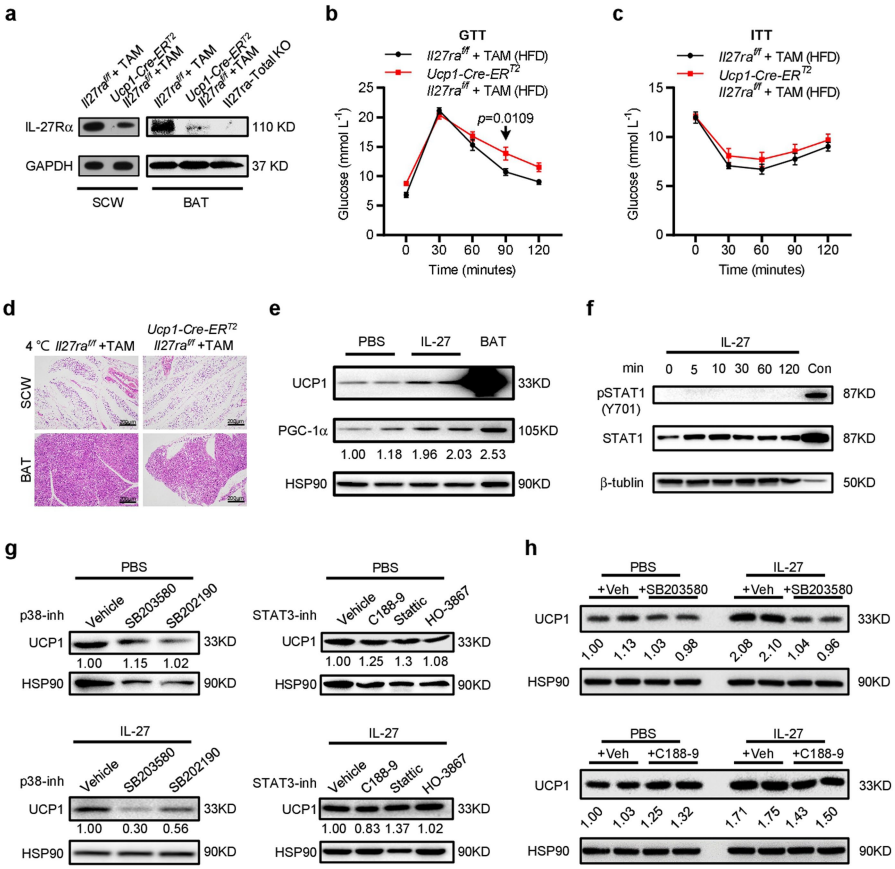


**Extended Data Fig. 7 | IL-27 upregulates UCP1 and improves the browning of subcutaneous white adipose tissue. a**. *Il27ra*$^{f/f}$ and *Ucp1-Cre-ER*$^{T2}$ *Il27ra*$^{f/f}$ mice at 8 weeks of age were i.p. injected with tamoxifen (2mg/mouse) for 4 times in a period of 7days, after another 7 days, SCWs and BATs were collected and used for immunoblot analysis of IL-27Rα expression. **b**&**c**. *Il27ra*$^{f/f}$ (n=10) and *Ucp1-Cre-ER*$^{T2}$ *Il27ra*$^{f/f}$ (n = 12) mice at 8 weeks of age were pre-treated with tamoxifen and then fed on HFD for 10 weeks. GTT (**b**, n = 10 for *Il27ra*$^{f/f}$ and n = 12 for *Ucp1-Cre-ER*$^{T2}$ *Il27ra*$^{f/f}$) and ITT (**c**, n = 9 for *Il27ra*$^{f/f}$ and n = 12 for *Ucp1-Cre-ER*$^{T2}$ *Il27ra*$^{f/f}$) were performed after 10 weeks of HFD treatment. **d**. *Il27ra*$^{f/f}$ and *Ucp1-Cre-ER*$^{T2}$ *Il27ra*$^{f/f}$ mice fed on normal chow were pre-treated with tamoxifen and then challenged at 4 °C for 12 hours, SCW and BAT were collected for histology analysis (H&E). Scale bar = 200μm. **e**. Primary beige adipocytes were generated *in vitro* from the SVF of WT SCW and then treated with rmIL-27 (100ng/ml) or PBS for 24 hours. Cells were lysed and protein extracts were used for Immunoblot analysis (each lane represents one biological independent sample). BAT tissue from WT mice was set as positive control. **f**. Immunoblot analysis of STAT1 phosphorylation in extracts from WT primary beige adipocytes treated with rmIL-27 (100ng/ml) for indicated time. IFN-γ (10ng/ml, 30 min) treated splenocytes were set as positive control (Con). **g**–**h**. Primary beige adipocytes from SCW of WT mice were generated *in vitro*. Two different p38 MAPK inhibitor (SB203580, 10μM and SB202190, 5μM) or three STAT3 inhibitor (C188-9, 10μM; stattic, 10μM or HO-3867, 20μM) were added into the culture medium 0.5 h before and in the duration of rmIL-27 treatment (100ng/ml for 12 h). The expression of UCP1 was detected via immunoblot. (**e**, **g** & **h**) Band densities were quantified with ImageJ and normalized. All experiments were repeated at least twice with similar results. Data are mean ± s.e.m. of biologically independent samples. Two-way ANOVA with Sidak's multiple comparisons test (**b** & **c**).

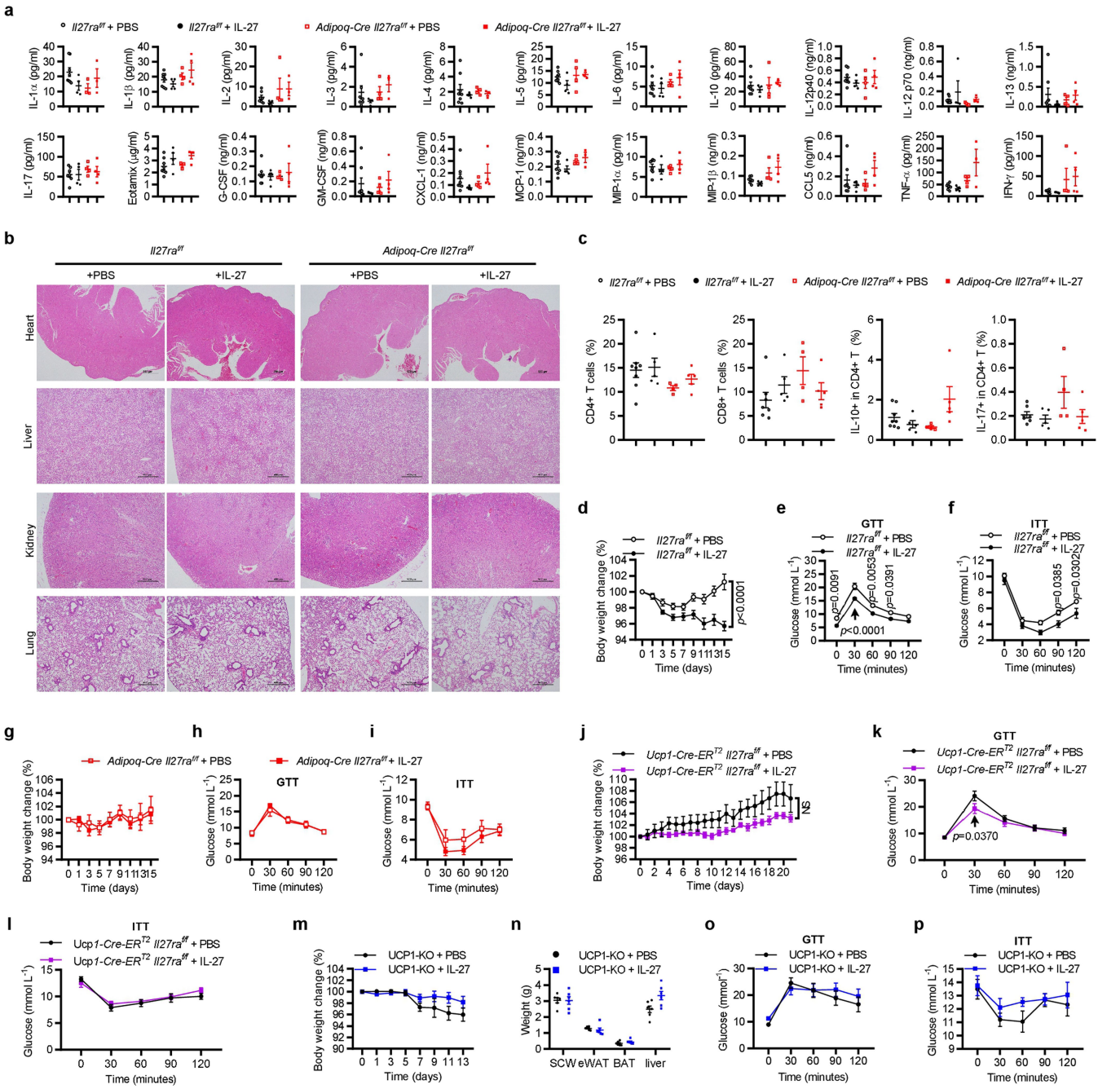


**Extended Data Fig. 8 | IL-27 promotes the activation of thermogenesis with promising therapeutic potential. a–i.** *Il27ra*$^{f/f}$ and *Adipoq-Cre Il27ra*$^{f/f}$ mice were fed on HFD for 32 weeks and then i.p. injected with rmIL-27 (100μg/kg) or PBS every other day for 15 days. **a.** Serum were collected and used for detection of inflammatory factors by Bio-Rad Bio-Plex 200 Multiplexing Analyzer System (n = 8 for *Il27ra*$^{f/f}$ + PBS, n=4 for *Adipoq-Cre Il27ra*$^{f/f}$ + PBS and all IL-27 treatment groups). **b.** Representative histological sections (H&E) of indicated tissues, scale bar = 500μm. **c.** The percentages of the infiltrating CD4 or CD8 T cells, and the cytokines production in CD4 T cells from liver were analysed by FACS (n = 8 for *Il27ra*$^{f/f}$ + PBS, n = 4 for *Adipoq-Cre Il27ra*$^{f/f}$ + PBS, n = 5 for IL-27 treatment groups). Body weight (**d**), GTT (**e**) and ITT (**f**) of *Il27ra*$^{f/f}$ mice were detected and recorded (n = 8 for PBS and n=5 for IL-27). Body weight (**g**), GTT (**h**) and ITT (**i**) of *Adipoq-Cre Il27ra*$^{f/f}$ mice were also detected and recorded (n = 4 for PBS and n=5 for IL-27). **j–l.** *Ucp1-Cre-ER*$^{T2}$ *Il27ra*$^{f/f}$ mice were fed on HFD for 12 weeks, pretreated with tamoxifen and then i.p. injected with rmIL-27 (100μg/kg) or PBS every other day for 21 days. The body weight (**j**), glucose tolerance test (**k**) and insulin tolerance test (**l**) were detected and recorded (n = 5 for PBS and n = 6 for IL-27). **m–p.** UCP1 KO mice were fed on HFD for 20 weeks and then i.p. injected with rmIL-27 (100μg/kg) or PBS every other day for 15 days. **m.** Body weight was recorded at indicated time points (n=6). **n.** The adipose tissues and livers were collected and weighted after 15 days of rmIL-27 treatment (n = 6). GTT (**o**, n = 6) and ITT (**p**, n = 4) were performed after 15 days of rmIL-27 treatment. All experiments were repeated at least twice with similar results. Data are mean ± s.e.m. of biologically independent samples. One-way ANOVA (**a** & **c**), two-way ANOVA (**d**, **g**, **j** & **m**); two-way ANOVA with Sidak's multiple comparisons test (**e**, **f**, **h**, **i**, **k**, **l**, **o** & **p**); two-tailed unpaired student's t-test (**n**).

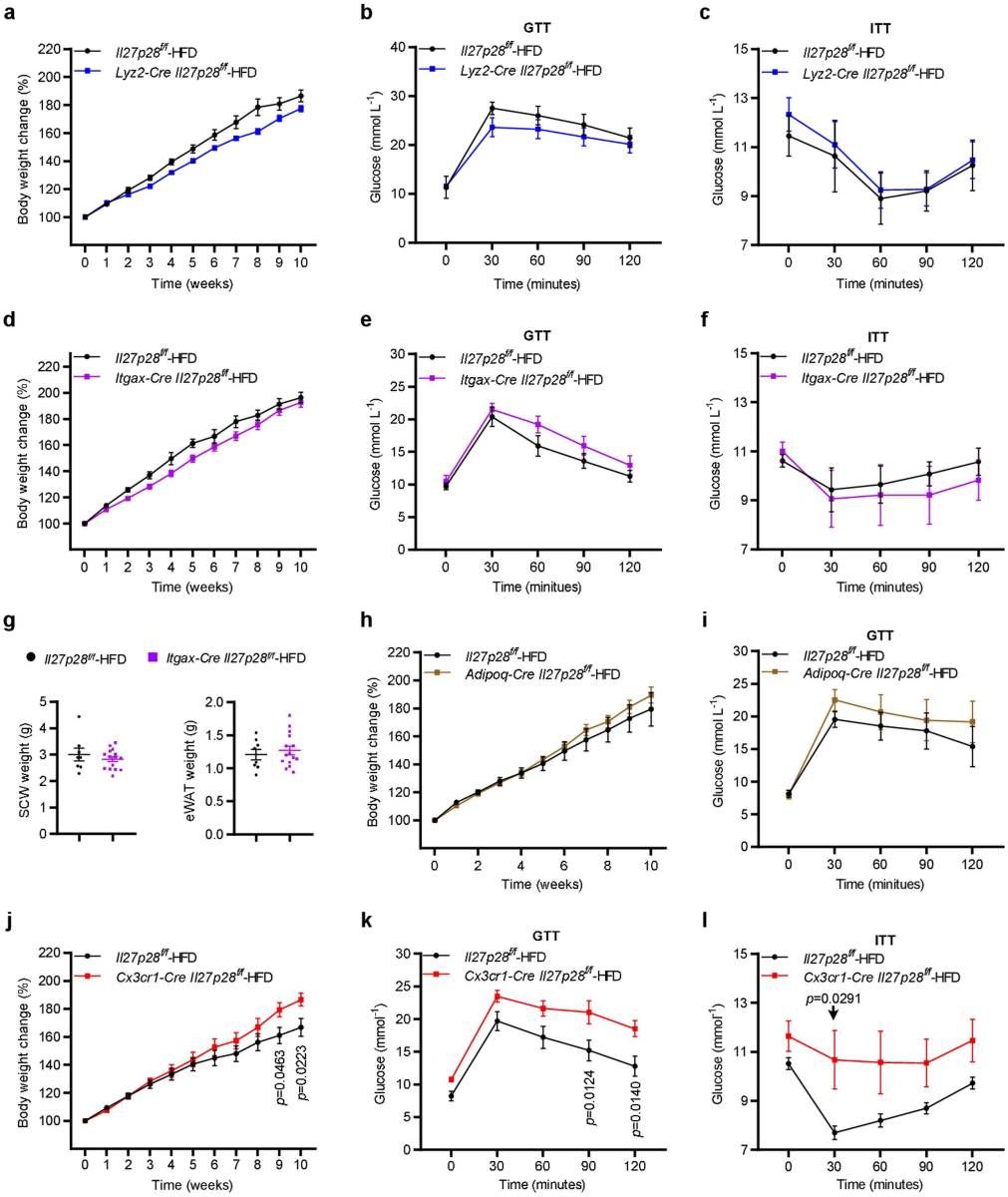


**Extended Data Fig. 9 | CX3CR1+ cells were an important source of IL-27 during HFD-induced obesity. a**–**c**. *Lyz2-Cre Il27p28*$^{f/f}$ and *Il27p28*$^{f/f}$ littermates at 8 weeks of age were treated with high fat diet (HFD) for 10 weeks. **a**. Body weight changes were recorded each week (n = 9 for *Il27p28*$^{f/f}$ and n = 6 for *Lyz2-Cre Il27p28*$^{f/f}$). Intraperitoneal GTT (**b**) and ITT (**c**) were performed after 10 weeks of treatment (n = 7 for *Il27p28*$^{f/f}$ and n = 6 for *Lyz2-Cre Il27p28*$^{f/f}$). **d**–**g**. *Itgax-Cre Il27p28*$^{f/f}$ and *Il27p28*$^{f/f}$ littermates at 8 weeks of age were fed on HFD for 10 weeks. Body weight changes were recorded each week (**d**, n = 8 for *Il27p28*$^{f/f}$ and n = 15 for *Itgax-Cre Il27p28*$^{f/f}$). Intraperitoneal GTT (**e**, n = 8 for *Il27p28*$^{f/f}$ and n = 15 for *Itgax-Cre Il27p28*$^{f/f}$) and ITT (**f**, n = 6) was performed after 10 weeks of treatment. **g**. Adipose tissues were collected and weighted after 10 weeks of HFD treatment (n = 8 for *Il27p28*$^{f/f}$ and n = 15 for *Itgax-Cre Il27p28*$^{f/f}$). **h**&**i**. *Adipoq-Cre Il27p28*$^{f/f}$ and *Il27p28*$^{f/f}$ littermates at 8 weeks of age were fed on HFD for 10 weeks. **h**. Body weight was recorded each week (n = 6). **i**. Intraperitoneal GTT was performed after 10 weeks of treatment (n = 6). **j**–**l**. *Cx3cr1-Cre Il27p28*$^{f/f}$ and *Il27p28*$^{f/f}$ littermates at 8 weeks of age were fed on HFD for 10 weeks. **j**. Body weight was recorded each week (n = 8). Intraperitoneal GTT (**k**) and ITT (**l**) were performed after 10 weeks of treatment (n = 8). All experiments were repeated at least twice with similar results. Data are mean ± s.e.m. of biologically independent samples. Two-way ANOVA (**a**, **d** & **h**); two-way ANOVA with Sidak's multiple comparisons test (**b**, **c**, **e**, **f** & **i**–**l**); two-tailed unpaired student's t-test (**g**).

nature portfolio

Corresponding author(s): Zhinan Yin, Richard A Flavell, Hengwen Yang, Ligong Lu

Last updated by author(s): Oct 1, 2021

# Reporting Summary

Nature Portfolio wishes to improve the reproducibility of the work that we publish. This form provides structure for consistency and transparency in reporting. For further information on Nature Portfolio policies, see our Editorial Policies and the Editorial Policy Checklist.

## Statistics

For all statistical analyses, confirm that the following items are present in the figure legend, table legend, main text, or Methods section.

| n/a | Confirmed | |
|---|---|---|
| ☐ | ☒ | The exact sample size (*n*) for each experimental group/condition, given as a discrete number and unit of measurement |
| ☐ | ☒ | A statement on whether measurements were taken from distinct samples or whether the same sample was measured repeatedly |
| ☐ | ☒ | The statistical test(s) used AND whether they are one- or two-sided<br>*Only common tests should be described solely by name; describe more complex techniques in the Methods section.* |
| ☒ | ☐ | A description of all covariates tested |
| ☐ | ☒ | A description of any assumptions or corrections, such as tests of normality and adjustment for multiple comparisons |
| ☐ | ☒ | A full description of the statistical parameters including central tendency (e.g. means) or other basic estimates (e.g. regression coefficient) AND variation (e.g. standard deviation) or associated estimates of uncertainty (e.g. confidence intervals) |
| ☐ | ☒ | For null hypothesis testing, the test statistic (e.g. *F*, *t*, *r*) with confidence intervals, effect sizes, degrees of freedom and *P* value noted<br>*Give P values as exact values whenever suitable.* |
| ☒ | ☐ | For Bayesian analysis, information on the choice of priors and Markov chain Monte Carlo settings |
| ☒ | ☐ | For hierarchical and complex designs, identification of the appropriate level for tests and full reporting of outcomes |
| ☒ | ☐ | Estimates of effect sizes (e.g. Cohen's *d*, Pearson's *r*), indicating how they were calculated |

*Our web collection on statistics for biologists contains articles on many of the points above.*

## Software and code

Policy information about availability of computer code

| | |
|---|---|
| Data collection | Comprehensive Laboratory Animal Monitoring System (CLAMS, Columbus Instruments, Columbus, OH) metabolic cages, Bio-rad ChemiDoc XRS, Bio-rad CFX96, Bio-rad Bio-Plex 200, Seahorse XF24 and BD FACS VERSE. |
| Data analysis | Flowjo V10, Image-Pro Plus V6.0 and Graphpad prism V8 |

For manuscripts utilizing custom algorithms or software that are central to the research but not yet described in published literature, software must be made available to editors and reviewers. We strongly encourage code deposition in a community repository (e.g. GitHub). See the Nature Portfolio guidelines for submitting code & software for further information.

## Data

Policy information about availability of data

All manuscripts must include a data availability statement. This statement should provide the following information, where applicable:

- Accession codes, unique identifiers, or web links for publicly available datasets
- A description of any restrictions on data availability
- For clinical datasets or third party data, please ensure that the statement adheres to our policy

A Data availability statement was added. The RNA-seq data for this work were deposited in the Sequence Read Archive (SRA) repository at NCBI under the accession number SRX10969398-10969403

# Field-specific reporting

Please select the one below that is the best fit for your research. If you are not sure, read the appropriate sections before making your selection.

☒ Life sciences ☐ Behavioural & social sciences ☐ Ecological, evolutionary & environmental sciences

For a reference copy of the document with all sections, see nature.com/documents/nr-reporting-summary-flat.pdf

# Life sciences study design

All studies must disclose on these points even when the disclosure is negative.

| | |
|---|---|
| Sample size | No statistical methods were used to predetermine sample size.<br>The sample size chosen for our animal experiments in this study was estimated based on our prior experience of performing similar sets of experiments (PMID: 22297845).<br>For human sample studies, we chose our sample size to give sufficient data values to conduct standard statistical tests.<br>No other experiments were carried out in this work. |
| Data exclusions | No data were excluded for data analysis applied |
| Replication | Data were representative of at least two independent replications. All attempts of replication were successful. |
| Randomization | For human studies, subjects were divided to two groups based on their BMI (Lean 18-25, Obese over 25).<br>For all other experiments, samples/animals were randomly allocated to experimental groups and processed. |
| Blinding | Investigators were not blinded for all the experiments since all the data were collected by experimental instruments other than human evaluation. |

# Reporting for specific materials, systems and methods

We require information from authors about some types of materials, experimental systems and methods used in many studies. Here, indicate whether each material, system or method listed is relevant to your study. If you are not sure if a list item applies to your research, read the appropriate section before selecting a response.

## Materials & experimental systems

| n/a | Involved in the study |
|---|---|
| ☐ | ☒ Antibodies |
| ☒ | ☐ Eukaryotic cell lines |
| ☒ | ☐ Palaeontology and archaeology |
| ☐ | ☒ Animals and other organisms |
| ☐ | ☒ Human research participants |
| ☒ | ☐ Clinical data |
| ☒ | ☐ Dual use research of concern |

## Methods

| n/a | Involved in the study |
|---|---|
| ☒ | ☐ ChIP-seq |
| ☐ | ☒ Flow cytometry |
| ☒ | ☐ MRI-based neuroimaging |

## Antibodies

| | |
|---|---|
| Antibodies used | Anti-pAKT (S473) mAb (Cat: 4060, Clone: D9E), anti-mouse AKT mAb (Cat: 4685, Clone: 11E7), anti-GAPDH mAb (Cat: 5174, Clone: D16H11), anti-HSP90 mAb (Cat: 4877, Clone: C45G5), anti-PPARγ mAb (Cat: 2435, Clone: C26H12), anti-mouse pSTAT3 (Y705) mAb (Cat: 9145, Clone: D3A7), anti-STAT3 mAb (Cat: 9139, Clone: 124H6), anti-p-p38 MAPK (T180/Y182) (Cat: 9211, polyclonal), anti-p38 MAPK (Cat: 9212, polyclonal), anti-pSTAT1 (Y701) mAb (Cat: 9167, Clone: 58D6), anti-STAT1 mAb (Cat: 14994, Clone: D1K9Y), anti-pATF2 (T71) (Cat: 9221, polyclonal), anti-ATF2 mAb (Cat: 35031, Clone: D4L2X) were purchased from Cell Signaling Technology. Anti-UCP1 (Cat: ab10983, polyclonal), anti-mouse UCP1 mAb (Cat: ab209483, Clone: EPR20381), anti-PGC-1α (Cat: ab54481, polyclonal), anti-PPARα (Cat: ab24509, polyclonal), anti-mouse IL-27Rα mAb (Cat: ab220359, Clone: EPR20863-3, 110kDa), anti-IL-27Rα (Cat: ab5997, polyclonal, 70kDa) were purchased from Abcam. Anti-β-actin mAb (Cat: 66009-1, Clone: 2D4H5) and anti-β-tubulin mAb (Cat: 66240-1, Clone: 1D4A4) were purchased from Proteintech. APC/CY7-anti-mouse CD45 (Cat: 557659, Clone: 30-F11), BV510-anti-mouse CD45.2 (Cat: 740131, Clone: 104) and PE/CY7-anti-mouse CD11b (Cat: 552850, Clone: M1/70) were purchased from BD Biosciences. PE-anti-mouse F4/80 (Cat: M100F1-09B, Clone: BM8), PE-anti-mouse CD8α (Cat: M10081-09B, Clone: 53.6.7), PE-anti-mouse IL-17 (Cat: M100I17-09B, Clone: 17F3), APC-anti-mouse IFN-γ (Cat: M100I16-11A, Clone: XMG1.2) were purchased from Sungene Biotech (Tianjin, China). PerCP/CY5.5-anti-mouse CD4 (Cat: 100434, Clone: GK1.5), FITC-anti-mouse CD19 (Cat: 152404, Clone: 1D3/CD19), APC/CY7-anti-mouse CD45.1 (Cat: 110716, Clone: A20), FITC-anti-mouse CD8α (Cat: 100706, Clone: 53.6.7), BV421-anti-mouse IL-10 (Cat: 505022, Clone: JES5-16E3), PE/CY7-anti-mouse CD3 (Cat: 100220, Clone: 17A2) and Alexa Fluro 647-anti-mouse F4/80 (Cat: 123122, Clone: BM8) were purchased from Biolegend. |
| Validation | Anti-pAKT (S473) mAb (Cat: 4060, Clone: D9E, WB, mouse, Dilution: 1:2000); https://www.cellsignal.com/products/primary-antibodies/phospho-akt-ser473-d9e-xp-rabbit-mab/4060. |

anti-mouse AKT mAb (Cat: 4685, Clone: 11E7, WB, mouse, Dilution: 1:1000); https://www.cellsignal.com/products/primary-antibodies/akt-pan-11e7-rabbit-mab/4685.
anti-GAPDH mAb (Cat: 5174, Clone: D16H11, WB, mouse, Dilution: 1:1000); https://www.cellsignal.com/products/primary-antibodies/gapdh-d16h11-xp-rabbit-mab/5174.
anti-HSP90 mAb (Cat: 4877, Clone: C45G5, WB, mouse, Dilution: 1:1000); https://www.cellsignal.com/products/primary-antibodies/hsp90-c45g5-rabbit-mab/4877.
anti-PPARγ mAb (Cat: 2435, Clone: C26H12, WB, mouse, Dilution: 1:1000); https://www.cellsignal.com/products/primary-antibodies/pparg-c26h12-rabbit-mab/2435.
anti-mouse pSTAT3 (Y705) mAb (Cat: 9145, Clone: D3A7, WB, mouse, Dilution: 1:2000); https://www.cellsignal.com/products/primary-antibodies/phospho-stat3-tyr705-d3a7-xp-rabbit-mab/9145.
anti-STAT3 mAb (Cat: 9139, Clone: 124H6, WB, mouse, Dilution: 1:1000); https://www.cellsignal.com/products/primary-antibodies/stat3-124h6-mouse-mab/9139.
anti-p-p38 MAPK (T180/Y182) (Cat: 9211, polyclonal, WB, mouse, Dilution: 1:1000); https://www.cellsignal.com/products/primary-antibodies/phospho-p38-mapk-thr180-tyr182-antibody/9211.
anti-p38 MAPK (Cat: 9212, polyclonal, WB, mouse, Dilution: 1:1000); https://www.cellsignal.com/products/primary-antibodies/p38-mapk-antibody/9212.
anti-pSTAT1 (Y701) mAb (Cat: 9167, Clone: 58D6, WB, mouse, Dilution: 1:1000); https://www.cellsignal.com/products/primary-antibodies/phospho-stat1-tyr701-58d6-rabbit-mab/9167.
anti-STAT1 mAb (Cat: 14994, Clone: D1K9Y, WB, mouse, Dilution: 1:1000); https://www.cellsignal.com/products/primary-antibodies/stat1-d1k9y-rabbit-mab/14994.
anti-pATF2 (T71) (Cat: 9221, polyclonal, WB, mouse, Dilution: 1:1000); https://www.cellsignal.com/products/primary-antibodies/phospho-atf-2-thr71-antibody/9221.
anti-ATF2 mAb (Cat: 35031, Clone: D4L2X, WB, mouse, Dilution: 1:1000); https://www.cellsignal.com/products/primary-antibodies/atf-2-d4l2x-xp-rabbit-mab/35031.
Anti-UCP1 (Cat: ab10983, polyclonal, WB, mouse, Dilution: 1:1000); https://www.abcam.com/ucp1-antibody-ab10983.html.
anti-mouse UCP1 mAb (Cat: ab209483, Clone: EPR20381, WB, mouse, Dilution: 1:1000); https://www.abcam.com/ucp1-antibody-epr20381-ab209483.html.
anti-PGC-1α (Cat: ab54481, polyclonal, WB, mouse, Dilution: 1:1000); https://www.abcam.com/pgc1-alpha-antibody-bsa-and-azide-free-ab54481.html.
anti-PPARα (Cat: ab24509, polyclonal, WB, mouse, Dilution: 1:100); https://www.abcam.com/ppar-alpha-antibody-ab24509.html.
anti-mouse IL-27Rα mAb (Cat: ab220359, Clone: EPR20863-3, 110kDa, mouse); IF (Dilution: 1:100) in this study and WB (Dilution: 1:1000) at https://www.abcam.com/wsx-1-antibody-epr20863-3-ab220359.html.
anti-IL-27Rα (Cat: ab5997, polyclonal, 70kDa, WB, mouse in this study, Dilution: 1:1000).
Anti-β-actin mAb (Cat: 66009-1, Clone: 2D4H5, WB, mouse, Dilution: 1:5000); https://www.ptglab.com/products/Pan-Actin-Antibody-66009-1-Ig.htm.
anti-β-tubulin mAb (Cat: 66240-1, Clone: 1D4A4, WB, mouse, Dilution: 1:10000); https://www.ptglab.com/products/Tubulin-beta-Antibody-66240-1-Ig.htm.
APC/CY7-anti-mouse CD45 (Cat: 557659, Clone: 30-F11, FACS, mouse, Dilution: 1:200); https://www.bdbiosciences.com/en-us/products/reagents/flow-cytometry-reagents/research-reagents/single-color-antibodies-ruo/apc-cy-7-rat-anti-mouse-cd45.561037.
BV510-anti-mouse CD45.2 (Cat: 740131, Clone: 104, FACS, mouse, Dilution: 1:200); https://www.bdbiosciences.com/en-sg/products/reagents/flow-cytometry-reagents/research-reagents/single-color-antibodies-ruo/bv510-mouse-anti-mouse-cd45-2.740131.
PE/CY7-anti-mouse CD11b (Cat: 552850, Clone: M1/70, FACS, mouse, Dilution: 1:200); https://www.bdbiosciences.com/en-us/products/reagents/flow-cytometry-reagents/research-reagents/single-color-antibodies-ruo/pe-cy-7-rat-anti-cd11b.552850.
PE-anti-mouse F4/80 (Cat: M100F1-09B, Clone: BM8, FACS, mouse, Dilution: 1:200); http://www.sungenebiotech.com/index.php?m=Product&a=product_xq&catid=2&proid=63&id=442.
PE-anti-mouse CD8α (Cat: M10081-09B, Clone: 53.6.7, FACS, mouse, Dilution: 1:200); http://sungenebiotech.com/index.php?m=Product&a=product_xq&catid=2&proid=51&prid=63&pid=36&id=71.
PE-anti-mouse IL-17 (Cat: M100I17-09B, Clone: 17F3, FACS, mouse, Dilution: 1:200); http://sungenebiotech.com/index.php?m=Product&a=product_xq&catid=2&proid=51&prid=63&pid=244&id=487.
APC-anti-mouse IFN-γ (Cat: M100I16-11A, Clone: XMG1.2, FACS, mouse, Dilution: 1:200); http://sungenebiotech.com/index.php?m=Product&a=product_xq&catid=2&proid=51&prid=63&pid=250&id=499.
PerCP/CY5.5-anti-mouse CD4 (Cat: 100434, Clone: GK1.5, FACS, mouse, Dilution: 1:200); https://www.biolegend.com/en-us/products/percp-cyanine5-5-anti-mouse-cd4-antibody-4220?GroupID=BLG4745.
FITC-anti-mouse CD19 (Cat: 152404, Clone: 1D3/CD19, FACS, mouse, Dilution: 1:200); https://www.biolegend.com/en-us/products/fitc-anti-mouse-cd19-antibody-13615.
APC/CY7-anti-mouse CD45.1 (Cat: 110716, Clone: A20, FACS, mouse, Dilution: 1:200); https://www.biolegend.com/en-us/products/apc-cyanine7-anti-mouse-cd45-1-antibody-2320.
FITC-anti-mouse CD8α (Cat: 100706, Clone: 53.6.7, FACS, mouse, Dilution: 1:200); https://www.biolegend.com/en-us/products/fitc-anti-mouse-cd8a-antibody-153.
BV421-anti-mouse IL-10 (Cat: 505022, Clone: JES5-16E3, FACS, mouse, Dilution: 1:200); https://www.biolegend.com/en-us/products/brilliant-violet-421-anti-mouse-il-10-antibody-7190.
PE/CY7-anti-mouse CD3 (Cat: 100220, Clone: 17A2, FACS, mouse, Dilution: 1:200); https://www.biolegend.com/en-us/products/pe-cyanine7-anti-mouse-cd3-antibody-6060.
Alexa Fluro 647-anti-mouse F4/80 (Cat: 123122, Clone: BM8, FACS, mouse, Dilution: 1:200); https://www.biolegend.com/en-us/products/alexa-fluor-647-anti-mouse-f4-80-antibody-4074.

## Animals and other organisms

Policy information about studies involving animals; ARRIVE guidelines recommended for reporting animal research

Laboratory animals

IL-27Ra KO (B6N.129P2-Il27ratm1Mak/J, Stock No: 018078), EBI-3 KO (B6.129X1-Ebi3tm1Rsb/J, Stock No: 008691), UCP1 KO (B6.129-Ucp1tm1Kz/J, Stock No: 003124), Cd2-Cre (B6.Cg-Tg(CD2-icre)4Kio/J, Stock No: 008520), Lyz2-Cre (B6.129P2-Lyz2tm1(cre)Ifo/J, Stock No:004781), Itgax-Cre (B6.Cg-Tg(Itgax-cre)1- 1Reiz/J, Stock No:008068), Cx3cr1-Cre (B6J.B6N(Cg)-Cx3cr1tm1.1(cre)Jung/J, Stock No: 025524), C57BL/6J (Stock No: 000664) and Adipoq-Cre (B6.FVB-Tg(Adipoq-cre) 1Evdr/J, Stock No: 028020) mice were purchased from The Jackson Laboratory. Ucp1-CreERT2 mice were provided from Dr. Christian Wolfrum (ETH Zurich) via Dr. Xiaoyong Yang (Yale

| | |
|---|---|
| | University). Il27raf/f (this paper) and Il27p28f/f mice were generated in our lab. Animal experiments were performed according to ethical regulations and protocols approved by the Institutional Animal Care and Use Committee of Jinan University and the Institutional Animal Care and Use Committee of Yale University. All experiments used sex and age-matched mice group housed at four to six animals per cage. The animal studies in this work have been carried out on either sex and yield consistent results. Randomization was performed in IL-27 therapy experiments and in generating bone marrow chimera. Mice were group housed in a temperature- and humidity-controlled (40%〜60% relative humidity), specific pathogen free animal facility at 25 °C under a 12:12-h light: dark cycle with free access to food and water. For diet study, mice at 8 weeks of age were fed a 60% high-fat diet (Research Diets, D12492) for indicated times. Mice body weights were measured every week. |
| Wild animals | No wild animals were used in this study. |
| Field-collected samples | No Field-collected samples were used in this study. |
| Ethics oversight | Animal experiments were performed according to ethical regulations and protocols approved by the Institutional Animal Care and Use Committee of Jinan University and the Institutional Animal Care and Use Committee of Yale University. |

Note that full information on the approval of the study protocol must also be provided in the manuscript.

## Human research participants

Policy information about studies involving human research participants

| | |
|---|---|
| Population characteristics | We recruited 42 obese individuals (BMI, 38.92 ± 1.349 kg/m2, data are mean ± s.e.m.), and 30 lean controls (BMI, 20.69 ± 0.3144 kg/m2). The information of characteristics for the human cohorts were shown in Supplementary Table 1. 7 of the obese subjects (BMI between 37 and 51) were underwent Roux En Y Gastric Bypass surgery (RYGB). The characteristics before and after surgery of each patient were shown in Supplementary Table 3. Bariatric procedures were performed laparoscopically by one single surgeon. Participants who were undergone RYGB were evaluated by surgical dietitian treatment. We also recruited 12 subjects that were diagnosed with type II diabetes and the information of characteristics were shown in Supplementary Table 2. |
| Recruitment | We recruited 42 obese individuals (BMI, 38.92 ± 1.349 kg/m2, data are mean ± s.e.m.), and 30 lean controls (BMI, 20.69 ± 0.3144 kg/m2). 7 of the obese subjects (BMI between 37 and 51) were underwent Roux En Y Gastric Bypass surgery (RYGB). We also recruited 12 subjects that were diagnosed with type 2 diabetes. The exclusion criteria for recruitment were: hypertension; abdominal surgery; previous bariatric surgery; virus hepatitis; colitis; gastrointestinal disease and gastrointestinal surgery within 5 years before recruitment and abnormal liver and kidney function. All subjects were weighed in light clothing without shoes. Body height and weight were measured by a height-weight scale, and BMI (kilograms per square meter) was calculated. No self-selection bias during the recruitment in this study. |
| Ethics oversight | Human research was approved by at the Institutional Review Board of the First Affiliated Hospital of Jinan University and was performed in accordance with the principle of the Helsinki Declaration II. A written informed consent was obtained from each participant. |

Note that full information on the approval of the study protocol must also be provided in the manuscript.

## Flow Cytometry

### Plots

Confirm that:

☒ The axis labels state the marker and fluorochrome used (e.g. CD4-FITC).

☒ The axis scales are clearly visible. Include numbers along axes only for bottom left plot of group (a 'group' is an analysis of identical markers).

☒ All plots are contour plots with outliers or pseudocolor plots.

☒ A numerical value for number of cells or percentage (with statistics) is provided.

### Methodology

| | |
|---|---|
| Sample preparation | Epididymal white adipose tissue was minced and digested as mentioned above. SVF pellets were used for surface staining of indicated molecules. After 15 min incubation, cells were washed by PBS and analyzed using BD FACSVerse Flow Cytometer (BD). The peripheral blood, inguinal lympho-nodes, spleen, liver, BAT and SCW from Bone marrow chimeric mice were collected and used for isolation of immune cells or SVF pellets. Cells were stained with APC-CY7-anti-mouse CD45.1, BV510-anti-mouse CD45.2, FITC-anti-mouse CD19, PerCP/CY5.5-anti-mouse CD4, PE-anti-mouse CD8alpha, Alexa Fluro 647-anti-mouse F4/80. After 15 min incubation, cells were washed by PBS and analyzed using BD FACSVerse Flow Cytometer. |
| Instrument | BD FACSVerse Flow Cytometer (BD) |
| Software | Flowjo-V10 |
| Cell population abundance | The abundance of cell populations was presented in the graphs in Extended Data Figure 2e, Extended Data Figure 5a and Extended Data Figure 7c. |

Gating strategy

A FSC-H/FSC-A gate was used to determine single-cell populations. The boundaries between "positive" and "negative" were determined by the clear cell subpopulations and unstained negative controls.

☒ Tick this box to confirm that a figure exemplifying the gating strategy is provided in the Supplementary Information.